Noiseless robust performance with structured uncertainties and initial state error

E. Jonckheere, *Life Fellow, IEEE* S. G. Schirmer, *Member, IEEE*, F. C. Langbein, *Member, IEEE*, C. A. Weidner

***Abstract*— A novel method to quantify robust performance is formulated for situations where structured parameter variations and initial state errors rather than extraneous noise are the main performance limiting factors. Parameter uncertainty is ubiquitous in classical control, as well as in quantum control where initial state preparation errors are prevalent. The central mathematical object is the error dynamics, the difference between nominal and perturbed dynamics, driven by the unperturbed or perturbed state, rather than an artificially imposed noise. The unperturbed versus perturbed dichotomy has the interpretation of the relative error dynamics scaled by either the unperturbed or perturbed dynamics. The unperturbed-driven error formulation follows the conventional lines of robust performance, but has the unique feature of decoupling the effect of the physically meaningful uncertainties from some artificial noise. However, the case of perturbed-driven error dynamics is a significant departure from conventional robustness in that it offers the possibility to side-step structured singular value computation. Applications to a lightly damped mechanical system and a slowly dephasing quantum system demonstrate the usefulness of the concepts across a broad range of systems. Finally, a fixed point algorithm specifically developed for quantum systems with state transitions depending in a nonlinear fashion on uncertainties is proposed as the substitute for classical μ.**

***Index Terms*— Uncertain systems, robust control, H-infinity control, quantum control.**

I. Introduction

Robust control problems are conveniently formulated as parametrically uncertain dynamics driven by extraneous noise where performance is assessed by the noise to output-to-be-controlled transmission. This raises the question whether the performance is limited by physically present noise, or whether noise is just a convenient way to deal with uncertainties in the dynamics governing the system. In addition, other potential sources of error such as in the initial state, not commonly considered in classical robustness, are relevant for certain applications. This particularly applies to quantum control, where, e.g., the fidelity of quantum state transfer is degraded by initial state preparation errors [3]. We propose a novel robust performance formulation that is independent of extraneous noise and incorporates initial state errors quite naturally.

The formulation is based on the error dynamics, the difference between the perturbed dynamics and the unperturbed dynamics. Here, *perturbed* is meant to denote the dynamics resulting from parameters deviating from their nominal, *unperturbed* values in a structured way as formalized in the structured singular value, or μ, analysis [25]. The error dynamics can be scaled relative to either (a) the unperturbed dynamics or (b) the perturbed dynamics. We develop and explore both paradigms. While (a) may be the most natural choice as the unperturbed dynamics is assumed to be known, scaling the error relative to the real perturbed dynamics can be advantageous in certain settings such as adaptive closed-loop control. Moreover, the latter is computationally simplified and sometimes offers less conservative results than the unperturbed case, but it deviates from the classical robust performance [25]. We illustrate the general unperturbed versus perturbed dichotomy on a benchmark mechanical example, and then specialize it to a robust quantum control problem [13] that motivates the alternative fixed point approach to μ computations.

The paper is organized as follows. In Sec. II two formulations of the error dynamics relative to the perturbed and unperturbed system dynamics are presented. Robust performance with respect to the dynamics of the unperturbed system is developed in Sec. III, starting with the most common case where no initial state preparation error and no uncertainty in the observation are present, and then adding these effects as additional performance limiting effects. In Sec. IV the performance is analyzed relative to the perturbed dynamics. In Sec. V we apply the results to a simple mechanical system. Finally, in Sec. VI we consider a quantum mechanical example.

II. Relative error dynamics

A. General formulation

We start with a system described by a model without uncertainties. The system dynamics resulting from the model are referred to as the *unperturbed* system dynamics. The dynamics of the real system, which deviates from the model

This research was supported in part by NSF Grant IRES-1829078.

EAJ is with the Department of Electrical and Computer Engineering, University of Southern California, Los Angeles, CA 90089 USA (e-mail: jonckhee@usc.edu).

SGS is with the Faculty of Science & Engineering, Swansea University, Swansea SA2 8PP, UK (e-mail: s.m.shermer@gmail.com).

FCL is with the School of Computer Science and Informatics, Cardiff University, Cardiff CF24 3AA, UK (e-mail: frank@langbein.org).

CAW is with the Quantum Engineering Technology Laboratories, H. H. Wills Physics Laboratory and Department of Electrical and Electronic Engineering, University of Bristol, Bristol BS8 1FD, United Kingdom (e-mail: c.weidner@bristol.ac.uk).

dynamics, is referred to as the *perturbed* system dynamics. Formulating the dynamics in terms of the controllable state-space representations, where $\boldsymbol{r}_u(t)$ is the state of the unperturbed system (following nominal model dynamics), $\boldsymbol{r}_p(t)$ is the state of the perturbed system, and $\boldsymbol{n}$ denotes external noise, we assume:

$$\begin{aligned} \tfrac{d}{dt}\boldsymbol{r}_u &= \boldsymbol{A}\boldsymbol{r}_u + \boldsymbol{B}\boldsymbol{n}, \qquad \boldsymbol{r}_u(0) = \boldsymbol{r}_{u,0}, \\ y_u &= \boldsymbol{C}_u\boldsymbol{r}_u; \end{aligned} \tag{1a}$$

$$\begin{aligned} \tfrac{d}{dt}\boldsymbol{r}_p &= (\boldsymbol{A}+\delta\boldsymbol{S})\boldsymbol{r}_p + \boldsymbol{B}\boldsymbol{n}, \quad \boldsymbol{r}_p(0) = \boldsymbol{r}_{p,0}, \\ y_p &= \boldsymbol{C}_p\boldsymbol{r}_p. \end{aligned} \tag{1b}$$

The multivariable controllable canonical form freezes the $\boldsymbol{B}$-matrix, so that the uncertainties are lumped into $\boldsymbol{A}$ and $\boldsymbol{C}$. The uncertainty in $\boldsymbol{A}$ is assumed to be structured with *structure* $\boldsymbol{S}$ and *magnitude* δ, while the uncertainty on $\boldsymbol{C}$ is left unstructured for now. A slight difficulty with the utilization of a controllable canonical form is that the same uncertain parameter could appear in both $\boldsymbol{A}$ and $\boldsymbol{C}$; this will be dealt with in Sec. III-B. State or output feedback to achieve specifications are assumed to be embedded in $\boldsymbol{A}$. In other words, Eqs. (1a) and (1b) represent the *closed-loop* system in its unperturbed and perturbed forms, resp. Extraneous noise $\boldsymbol{n}$ has been added for generality. The output error $\boldsymbol{e}(t) := \boldsymbol{C}_p\boldsymbol{r}_p - \boldsymbol{C}_u\boldsymbol{r}_u$ admits two different, but equivalent, state-space realizations, both of which have state $\boldsymbol{z}(t) := \boldsymbol{r}_p(t) - \boldsymbol{r}_u(t)$:

$$\begin{aligned} \tfrac{d}{dt}\boldsymbol{z} &= (\boldsymbol{A}+\delta\boldsymbol{S})\boldsymbol{z} + \delta\boldsymbol{S}\boldsymbol{w}_u, \qquad \boldsymbol{z}(0) = \boldsymbol{z}_0, \\ \boldsymbol{e} &= \boldsymbol{C}_p\boldsymbol{z} + (\boldsymbol{C}_p - \boldsymbol{C}_u)\boldsymbol{w}_u; \end{aligned} \tag{2a}$$

$$\begin{aligned} \tfrac{d}{dt}\boldsymbol{z} &= \boldsymbol{A}\boldsymbol{z} + \delta\boldsymbol{S}\boldsymbol{w}_p, \qquad \boldsymbol{z}(0) = \boldsymbol{z}_0, \\ \boldsymbol{e} &= \boldsymbol{C}_u\boldsymbol{z} + (\boldsymbol{C}_p - \boldsymbol{C}_u)\boldsymbol{w}_p. \end{aligned} \tag{2b}$$

The difference between the two models is in the driving terms: $\boldsymbol{w}_u := \boldsymbol{r}_u$ for the *unperturbed* error dynamics (2a) and $\boldsymbol{w}_p := \boldsymbol{r}_p$ for the *perturbed* error dynamics (2b). This entails different sources of potential instabilities: in the unperturbed formulation of Eq. (2a), assuming $\boldsymbol{w}_u \in L^2$, the instability is in the free dynamics $\boldsymbol{A}+\delta\boldsymbol{S}$; while in the perturbed case of Eq. (2b) the instability is in the input term $\boldsymbol{w}_p$ which need not be in L^2. Note that the noise term $\boldsymbol{B}\boldsymbol{n}$ has disappeared, but that the two models are subject to initial error $\boldsymbol{z}(0)$.

The state-space error dynamics gives the transfer matrices

$$\boldsymbol{T}^u_{\boldsymbol{e},\boldsymbol{w}_u}(s,\delta) := (\boldsymbol{C}_p - \boldsymbol{C}_u) + \boldsymbol{C}_p(s\boldsymbol{I} - \boldsymbol{A} - \delta\boldsymbol{S})^{-1}\delta\boldsymbol{S}, \tag{3a}$$

$$\boldsymbol{T}^p_{\boldsymbol{e},\boldsymbol{w}_p}(s,\delta) := (\boldsymbol{C}_p - \boldsymbol{C}_u) + \boldsymbol{C}_u(s\boldsymbol{I} - \boldsymbol{A})^{-1}\delta\boldsymbol{S}, \tag{3b}$$

where we have adopted the universal notation of $\boldsymbol{T}_{\boldsymbol{y},\boldsymbol{x}}$ to denote the transfer matrix from $\hat{\boldsymbol{x}}$ to $\hat{\boldsymbol{y}}$, and $\hat{\boldsymbol{x}}(s)$ denotes the Laplace transform of $\boldsymbol{x}(t)$. Application of the matrix inversion lemma reveals that $\boldsymbol{T}^u$ is the transfer function for the error scaled relative to the unperturbed dynamics, while $\boldsymbol{T}^p$ is scaled relative to the perturbed dynamics, as easily seen from

$$\begin{aligned} \boldsymbol{T}^u_{\boldsymbol{e},\boldsymbol{w}_u}(s,\delta) = &\left[\boldsymbol{C}_p(s\boldsymbol{I} - \boldsymbol{A} - \delta\boldsymbol{S})^{-1} - \boldsymbol{C}_u(s\boldsymbol{I} - \boldsymbol{A})^{-1}\right] \\ &\cdot \left[(s\boldsymbol{I} - \boldsymbol{A})^{-1}\right]^{-1}, \end{aligned} \tag{4a}$$

$$\begin{aligned} \boldsymbol{T}^p_{\boldsymbol{e},\boldsymbol{w}_p}(s,\delta) = &\left[\boldsymbol{C}_p(s\boldsymbol{I} - \boldsymbol{A} - \delta\boldsymbol{S})^{-1} - \boldsymbol{C}_u(s\boldsymbol{I} - \boldsymbol{A})^{-1}\right] \\ &\cdot \left[(s\boldsymbol{I} - \boldsymbol{A} - \delta\boldsymbol{S})^{-1}\right]^{-1}. \end{aligned} \tag{4b}$$

Moreover, Eqs. (4a) and (4b) reveal that the two models differ by a frequency correction factor:

$$\boldsymbol{T}^p_{\boldsymbol{e},\boldsymbol{w}_p}(s,\delta) = \boldsymbol{T}^u_{\boldsymbol{e},\boldsymbol{w}_u}(s,\delta)\left((s\boldsymbol{I} - \boldsymbol{A})^{-1}(s\boldsymbol{I} - \boldsymbol{A} - \delta\boldsymbol{S})\right). \tag{5}$$

Remark 1: It is important to distinguish two different interpretations of "unperturbed vs. perturbed." On the one hand, it could indicate whether the physical $\boldsymbol{r}_{u,p}$-dynamics are in their nominal or physically perturbed state and this distinction will be made precise by a subscript as in $\boldsymbol{w}_{u,p}$. On the other hand, it could also refer to the error model, which could be driven by the perturbed or the unperturbed dynamics, and will be specified by a superscript as in $\boldsymbol{T}^u$, $\boldsymbol{T}^p$.

Remark 2: Another dichotomy is the "absolute vs. relative" perturbation. In the above formulation, δ could be either an absolute or a relative magnitude; the difference resides in the structure matrix $\boldsymbol{S}$. While classically [2], [16] the sensitivity matrix relates the closed-loop perturbation to the open-loop perturbation in their relative values, whether relative or absolute perturbations ought to be considered depends on the context. For example, if the nominal parameter is 0, as is the case for the detuning parameter in our quantum control example, only the absolute perturbation makes sense; the same applies to the quantum initial state preparation error, the nominal value of which is 0 as well.

B. Main contributions of the paper

In this subsection, we briefly outline the key points addressed by this manuscript.

1) Departure from classical robust performance: The main contribution is that the robust performance is carried on Eqs. (4a), (4b), rather than on Eq. (1b), as usual. To put it another way, classical robust performance bounds $\|\boldsymbol{T}_{y_p,\boldsymbol{n}}(s,\delta)\|_\infty$ whereas here we bound $\|\boldsymbol{T}^{u,p}_{y_p-y_u,\boldsymbol{w}_{u,p}}(s,\delta)\|_\infty$. The latter still requires some μ-computations, but with some caveats, especially in the perturbed case that departs from the classical μ. With the fixed-point computation of μ that applies to nonlinear rather than affine perturbations, the breakup from classical structured singular value is complete.

2) "Noiseless" approach: $\|\boldsymbol{T}^{u,p}_{y_p-y_u,\boldsymbol{w}_{u,p}}(s,\delta)\|_\infty$ allows the objective assessment of the effect of the uncertainties, rather than their effect on the transmission of some arbitrarily inputted noise $\boldsymbol{n}$. Both the unperturbed and perturbed formulations are driven by *physically objective* driving terms: the states of the unperturbed and the perturbed dynamics, resp. Should some additive noise $\boldsymbol{n}$ be physically justifiable, then the same approach decouples the effect of the noise and allows performance to be assessed solely as a consequence of uncertain parameters.

3) Perturbed versus unperturbed scaling: Expansion with respect to the unperturbed state (case a) makes sense as we are expressing the scaled deviation of the dynamics (as captured by the error transfer function) in terms of something we know. Expansion with respect to the perturbed state (case b), however, is also interesting in that we are expressing how much the dynamics of the system deviates from the presumed dynamics in terms of the *actual* state of the system. This

is a more relevant formulation if we can probe the actual dynamics of the system experimentally. For a historical review of this unperturbed vs. perturbed scaling dichotomy see [16]. For oscillatory systems, such as lightly damped space structures [11], [12], or weakly decoherent quantum systems [6], [7], the unperturbed error dynamics has the advantage that the frequency sweep can be limited to the known eigenfrequencies of $\boldsymbol{A}$. The perturbed error dynamics still requires the classical frequency sweep because the eigenfrequencies of $\boldsymbol{A}+\delta\boldsymbol{S}$ are imprecisely known.

III. Robust performance in the unperturbed formulation

This section proceeds from Eq. (2a) with an *unperturbed* driving term $\hat{\boldsymbol{w}}_u$. We begin with the simplified case of zero initial state error, where parameter errors are lumped into $\boldsymbol{A}$. From there, we progressively build up to more complicated situations by adding initial state errors, uncertainties in $\boldsymbol{C}$, and various combination of uncertainties.

A. Zero initial condition error

Elementary matrix manipulation reveals that the transfer matrix $\boldsymbol{T}^u_{\boldsymbol{e},\boldsymbol{w}_u}$ in the formulation of Eq. (3a) is obtained from

$$\begin{bmatrix}\hat{\boldsymbol{v}}\\ \hat{\boldsymbol{e}}(s)\end{bmatrix}=\underbrace{\begin{bmatrix}\boldsymbol{\Phi}(s)^{-1}\boldsymbol{S} & \boldsymbol{\Phi}(s)^{-1}\boldsymbol{S}\\ \boldsymbol{C}_p & \boldsymbol{C}_p-\boldsymbol{C}_u\end{bmatrix}}_{\boldsymbol{G}_{\boldsymbol{e},\boldsymbol{w}_u}(s)}\begin{bmatrix}\hat{\boldsymbol{\eta}}\\ \hat{\boldsymbol{w}}_u(s)\end{bmatrix},\tag{6}$$

with $\boldsymbol{\Phi}(s)=s\boldsymbol{I}-\boldsymbol{A}$ and feedback $\hat{\boldsymbol{\eta}}=(\delta\boldsymbol{I})\hat{\boldsymbol{v}}$. With this feedback, we compute $\|\boldsymbol{T}^u_{\boldsymbol{e},\boldsymbol{w}_u}(s,\delta)\|$ via a *fictitious* feedback $\hat{\boldsymbol{w}}_u=\Delta_f\hat{\boldsymbol{e}}$, with Δ_f a complex fully populated matrix. Specifically, a simple singular value argument shows that

$$\|\boldsymbol{T}^u_{\boldsymbol{e},\boldsymbol{w}_u}(s,\delta)\|=1/\min\{\|\Delta_f\|:\det(\boldsymbol{I}-\boldsymbol{T}^u_{\boldsymbol{e},\boldsymbol{w}_u}(s,\delta)\Delta_f)=0\}.$$

To compute $\max_\delta\|\boldsymbol{T}^u_{\boldsymbol{e},\boldsymbol{w}_u}(s,\delta)\|$, subject to closed-loop stability, the two feedbacks are combined as

$$\begin{bmatrix}\hat{\boldsymbol{\eta}}\\ \hat{\boldsymbol{w}}_u\end{bmatrix}=\underbrace{\begin{bmatrix}\delta\boldsymbol{I} & 0\\ 0 & \boldsymbol{\Delta}_f\end{bmatrix}}_{\boldsymbol{\Delta}(\delta,\Delta_f)}\begin{bmatrix}\hat{\boldsymbol{v}}\\ \hat{\boldsymbol{e}}\end{bmatrix},\tag{7}$$

where $\boldsymbol{\Delta}$ defines the *structure* $\mathcal{D}$, i.e., the set of all block-diagonal matrices with the top left hand corner a real scalar matrix and the bottom left hand corner a fully populated complex matrix. It is readily verified that

$$\begin{aligned}&\det(\boldsymbol{I}-\boldsymbol{G}_{\boldsymbol{e},\boldsymbol{w}_u}(s)\boldsymbol{\Delta}(\delta,\boldsymbol{\Delta}_f))=\\ &\quad\det(\boldsymbol{I}-\boldsymbol{\Phi}^{-1}\boldsymbol{S}\delta)\det(\boldsymbol{I}-\boldsymbol{T}^u_{\boldsymbol{e},\boldsymbol{w}_u}(s,\delta)\boldsymbol{\Delta}_f),\end{aligned}\tag{8}$$

where the first factor relates to the closed-loop stability, as $\det(\boldsymbol{I}-\boldsymbol{\Phi}^{-1}\boldsymbol{S}\delta)=\det(\boldsymbol{\Phi}^{-1})\det(s\boldsymbol{I}-\boldsymbol{A}-\boldsymbol{S}\delta)$. With this material, the robust performance theorem [25, Th. 10.8] reads

Theorem 1: If $\boldsymbol{\Phi}(s)$ is invertible, then $\|\boldsymbol{T}^u_{\boldsymbol{e},\boldsymbol{w}_u}(s,\delta)\|\le\mu_{\mathcal{D}}(\boldsymbol{G}_{\boldsymbol{e},\boldsymbol{w}_u}(s)),\forall\ \delta<1/\mu_{\mathcal{D}}(\boldsymbol{G}_{\boldsymbol{e},\boldsymbol{w}_u}(s))$, where

$$\mu_{\mathcal{D}}(\boldsymbol{G}_{\boldsymbol{e},\boldsymbol{w}_u}(s))=\frac{1}{\min_{\boldsymbol{\Delta}\in\mathcal{D}}\{\|\boldsymbol{\Delta}\|:\det(\boldsymbol{I}-\boldsymbol{G}_{\boldsymbol{e},\boldsymbol{w}_u}(s)\boldsymbol{\Delta})=0\}}$$

is the structured singular value specific to $\mathcal{D}=\{\boldsymbol{\Delta}(\delta,\Delta_f)\}$.

1) Extensions: The above is a generic result that can easily be extended to more complicated uncertainty patterns. Given a transfer matrix $\boldsymbol{T}_{\boldsymbol{e},\boldsymbol{w}_g}(s,\delta_g)$ from a generalized disturbance to some error, subject to a generalized structured uncertainty of magnitude δ_g, the difficulty is to find a matrix $\boldsymbol{G}_g$ and a structured feedback $\boldsymbol{\Delta}_g$, such that wrapping the structured feedback $\hat{\boldsymbol{\eta}}_g=\boldsymbol{\Delta}_g\hat{\boldsymbol{v}}_g$ around

$$\begin{bmatrix}\hat{\boldsymbol{v}}_g\\ \hat{\boldsymbol{e}}\end{bmatrix}=\boldsymbol{G}_g\begin{bmatrix}\hat{\boldsymbol{\eta}}_g\\ \hat{\boldsymbol{w}}_g\end{bmatrix},$$

reproduces $\boldsymbol{T}_{\boldsymbol{e},\boldsymbol{w}_g}(s,\delta_g)$. In the subsections that follow, we derive $\boldsymbol{G}_g$ and $\boldsymbol{\Delta}_g$ and bound $\|\boldsymbol{T}_{\boldsymbol{e},\boldsymbol{w}_g}(s,\delta_g)\|$ without repeating the argument of Th. 1 with the objective of bounding $\boldsymbol{T}_{\boldsymbol{e},\boldsymbol{w}_g}(s,\delta_g)$ with

$$\mu_{\mathcal{D}}(\boldsymbol{G}_g(s))=\left[\min_{\boldsymbol{\Delta}\in\mathcal{D}}\{\|\boldsymbol{\Delta}\|:\det(\boldsymbol{I}-\boldsymbol{G}_g\boldsymbol{\Delta})=0\}\right]^{-1},$$

where $\mathcal{D}=\{\text{block-diag}(\boldsymbol{\Delta}_g,\boldsymbol{\Delta}_f)\}$.

B. Zero initial error and uncertain output matrix C

The preceding framework can be extended to account for uncertainty in the observations structured as

$$\boldsymbol{C}_p-\boldsymbol{C}_u=\delta_c\boldsymbol{S}_c.\tag{9}$$

Substitute $\delta_c\boldsymbol{S}_c$ for $\boldsymbol{C}_p-\boldsymbol{C}_u$ and $\boldsymbol{C}_u+\delta_c\boldsymbol{S}_c$ for $\boldsymbol{C}_p$ in Eq. (6); then pull δ_c out of the same equation via the feedback

$$\begin{bmatrix}\hat{\boldsymbol{\eta}}_2\\ \hat{\boldsymbol{\eta}}_3\end{bmatrix}=\delta_c\boldsymbol{I}\begin{bmatrix}\hat{\boldsymbol{v}}_2\\ \hat{\boldsymbol{v}}_3\end{bmatrix}\tag{10}$$

wrapped around

$$\begin{bmatrix}\hat{\boldsymbol{v}}_1\\ \hat{\boldsymbol{v}}_2\\ \hat{\boldsymbol{v}}_3\\ \hat{\boldsymbol{e}}\end{bmatrix}=\underbrace{\left[\begin{array}{c|cc|c}\boldsymbol{\Phi}^{-1}\boldsymbol{S} & 0 & 0 & \boldsymbol{\Phi}^{-1}\boldsymbol{S}\\ \hline \boldsymbol{I} & 0 & 0 & 0\\ 0 & 0 & 0 & \boldsymbol{I}\\ \hline \boldsymbol{C}_u & \boldsymbol{S}_c & \boldsymbol{S}_c & 0\end{array}\right]}_{\boldsymbol{G}^c_{\boldsymbol{e},\hat{\boldsymbol{w}}_u}}\begin{bmatrix}\hat{\boldsymbol{\eta}}_1\\ \hat{\boldsymbol{\eta}}_2\\ \hat{\boldsymbol{\eta}}_3\\ \hat{\boldsymbol{w}}_u\end{bmatrix}.\tag{11}$$

Eqs. (10) and (11) together (after eliminating $\hat{\boldsymbol{v}}_2$, $\hat{\boldsymbol{v}}_3$ and $\hat{\boldsymbol{\eta}}_2,\hat{\boldsymbol{\eta}}_3$ using Eq. (10)) reproduce Eq. (6), with the feedback $\hat{\boldsymbol{\eta}}_1=\delta\hat{\boldsymbol{v}}_1$ playing the same role as $\hat{\boldsymbol{\eta}}=(\delta\boldsymbol{I})\hat{\boldsymbol{v}}$. Therefore, Eqs. (10) and (11) reproduce $\boldsymbol{T}^u_{\boldsymbol{e},\boldsymbol{w}_u}(s,\delta,\delta_c)$ in the same manner as Eq. (6) with $\hat{\boldsymbol{\eta}}=(\delta\boldsymbol{I})\hat{\boldsymbol{v}}$ reproduces $T^u_{\boldsymbol{e},\boldsymbol{w}_u}(s,\delta)$.

To put it another way, from Eq. (6), observe that $\hat{\boldsymbol{\eta}}=\hat{\boldsymbol{z}}$ and

$$\hat{\boldsymbol{e}}=\boldsymbol{C}_u\hat{\boldsymbol{\eta}}+\boldsymbol{S}_c\delta_c\hat{\boldsymbol{\eta}}+\boldsymbol{S}_c\delta_c\hat{\boldsymbol{w}}_u.$$

To remove δ_c, we create a copy $\hat{\boldsymbol{v}}_2$ of $\hat{\boldsymbol{\eta}}_1=\hat{\boldsymbol{z}}$, feed it through δ_c to obtain $\hat{\boldsymbol{\eta}}_2=\delta_c\hat{\boldsymbol{z}}$, and also create a copy $\hat{\boldsymbol{v}}_3$ of $\hat{\boldsymbol{w}}_u$, feed it through δ_c, to obtain $\hat{\boldsymbol{\eta}}_3=\delta_c\hat{\boldsymbol{w}}_u$. With $\hat{\boldsymbol{\eta}}_2$, $\hat{\boldsymbol{\eta}}_3$, the above becomes

$$\hat{\boldsymbol{e}}=\boldsymbol{C}_u\hat{\boldsymbol{\eta}}_1+\boldsymbol{S}_c\hat{\boldsymbol{\eta}}_2+\boldsymbol{S}_c\hat{\boldsymbol{\eta}}_3;$$

that is, Eq. (11).

The overall feedback structure that defines the structure $\mathcal{D}$ for $\mu_{\mathcal{D}}$ is

$$\begin{bmatrix}\hat{\boldsymbol{\eta}}_1\\ \hat{\boldsymbol{\eta}}_2\\ \hat{\boldsymbol{\eta}}_3\\ \hat{\boldsymbol{w}}_u\end{bmatrix}=\underbrace{\left[\begin{array}{c|c|c|c}\delta\boldsymbol{I} & 0 & 0 & 0\\ \hline 0 & \delta_c\boldsymbol{I} & 0 & 0\\ \hline 0 & 0 & \delta_c\boldsymbol{I} & 0\\ \hline 0 & 0 & 0 & \boldsymbol{\Delta}_f\end{array}\right]}_{\boldsymbol{\Delta}(\delta,\delta_c,\delta_c,\boldsymbol{\Delta}_f)}\begin{bmatrix}\hat{\boldsymbol{v}}_1\\ \hat{\boldsymbol{v}}_2\\ \hat{\boldsymbol{v}}_3\\ \hat{\boldsymbol{e}}\end{bmatrix}.\tag{12}$$

We have the following

Theorem 2: $\|\boldsymbol{T}_{\boldsymbol{e},\boldsymbol{w}_u}(s,\delta,\delta_c)\| \leq \mu_{\mathcal{D}}(\boldsymbol{G}^c_{\boldsymbol{e},\hat{\boldsymbol{w}}_u}(s))$, for $\delta,\delta_c < [\mu_{\mathcal{D}}(\boldsymbol{G}^c_{\boldsymbol{e},\hat{\boldsymbol{w}}_u}(s))]^{-1}$, with $\mathcal{D}=\{\boldsymbol{\Delta}(\delta,\delta_c,\delta_c,\boldsymbol{\Delta}_f)\}$.

Remark 3: If the same uncertain parameter appears in both $\boldsymbol{A}$ and $\boldsymbol{C}$, the formulation remains valid subject to a mild modification. If $\boldsymbol{S}$ denotes the structure of the uncertainty in $\boldsymbol{A}$ and $\boldsymbol{S}_c$ the structure in $\boldsymbol{C}$, all that needs to be done is to equate δ and δ_c and the overall feedback becomes $\boldsymbol{\Delta}(\delta,\delta,\delta,\boldsymbol{\Delta}_f)$.

C. Effect of initial state preparation error

We further extend the framework to explicitly consider the effect of initial state preparation errors. Taking the Laplace transform of Eq. (2a) yields

$$(s\boldsymbol{I}-\boldsymbol{A}-\delta\boldsymbol{S})\hat{\boldsymbol{z}}(s)=\delta\boldsymbol{S}\hat{\boldsymbol{w}}_u(s)+\boldsymbol{z}(0), \tag{13a}$$

$$\hat{\boldsymbol{e}}(s)=\boldsymbol{C}_p\hat{\boldsymbol{z}}(s)+(\boldsymbol{C}_p-\boldsymbol{C}_u)\hat{\boldsymbol{w}}_u(s). \tag{13b}$$

To proceed, we look at how Eq. (6) should be augmented to incorporate an initial state error $\boldsymbol{z}(0)$. Recall that the crucial point of Eq. (6) is that $\hat{\boldsymbol{\eta}}$ is the $\hat{\boldsymbol{z}}$ response to $\hat{\boldsymbol{w}}_u$. Here, $\hat{\boldsymbol{\eta}}_1$ is the $\hat{\boldsymbol{z}}$ response to $\hat{\boldsymbol{w}}_u$. In the case of initial state error, we need to construct the $\hat{\boldsymbol{z}}$ response to $\boldsymbol{z}(0)$. The extended version of Eq. (6),

$$\begin{bmatrix}\hat{\boldsymbol{v}}_1\\ \hat{\boldsymbol{v}}_2\\ \hline \hat{\boldsymbol{v}}_3\\ \hline \hat{\boldsymbol{e}}\end{bmatrix}=\underbrace{\left[\begin{array}{cc|c|cc} \boldsymbol{\Phi}^{-1}\boldsymbol{S} & 0 & 0 & 0 & \boldsymbol{\Phi}^{-1}\boldsymbol{S}\\ 0 & \boldsymbol{\Phi}^{-1}\boldsymbol{S} & 0 & \boldsymbol{\Phi}^{-1} & 0\\ \hline 0 & \boldsymbol{\Phi}^{-1}\boldsymbol{S} & 0 & \boldsymbol{\Phi}^{-1} & 0\\ \hline \boldsymbol{C}_p & 0 & \boldsymbol{C}_p & 0 & \boldsymbol{C}_p-\boldsymbol{C}_u \end{array}\right]}_{G}\begin{bmatrix}\hat{\boldsymbol{\eta}}_1\\ \hat{\boldsymbol{\eta}}_2\\ \hline \hat{\boldsymbol{\eta}}_3\\ \hline \boldsymbol{z}(0)\\ \hat{\boldsymbol{w}}_u\end{bmatrix} \tag{14}$$

under the extended feedback structure

$$\begin{bmatrix}\hat{\boldsymbol{\eta}}_1\\ \hat{\boldsymbol{\eta}}_2\end{bmatrix}=\begin{bmatrix}\delta\boldsymbol{I} & 0\\ 0 & \delta\boldsymbol{I}\end{bmatrix}\begin{bmatrix}\hat{\boldsymbol{v}}_1\\ \hat{\boldsymbol{v}}_2\end{bmatrix},$$

precisely constructs the $\hat{\boldsymbol{z}}$ response to $\boldsymbol{z}(0)$ as $\hat{\boldsymbol{v}}_2$. The problem is that $\hat{\boldsymbol{v}}_2$ is at the output while it should be at the input to contribute to $\hat{\boldsymbol{e}}$. Putting $\hat{\boldsymbol{v}}_2$ at the input is accomplished by creating a copy of $\hat{\boldsymbol{v}}_2$, say $\hat{\boldsymbol{v}}_3$, and feeding it back to the input via $\hat{\boldsymbol{\eta}}_3=\boldsymbol{I}\hat{\boldsymbol{v}}_3$. To recover the classical robust performance formulation, this feedback needs to be absorbed in the $\boldsymbol{G}$-matrix. This is equivalent to eliminating $\hat{\boldsymbol{v}}_3=\hat{\boldsymbol{\eta}}_3$, which is done by observing that $\hat{\boldsymbol{v}}_3=\hat{\boldsymbol{\eta}}_3=\boldsymbol{\Phi}^{-1}\boldsymbol{S}\hat{\boldsymbol{\eta}}_2+\boldsymbol{\Phi}^{-1}\boldsymbol{z}(0)$. Putting this into Eq. (14) yields

$$\begin{bmatrix}\hat{\boldsymbol{v}}_1\\ \hat{\boldsymbol{v}}_2\\ \hline \hat{\boldsymbol{e}}\end{bmatrix}=\underbrace{\left[\begin{array}{cc|cc} \boldsymbol{\Phi}^{-1}\boldsymbol{S} & 0 & 0 & \boldsymbol{\Phi}^{-1}\boldsymbol{S}\\ 0 & \boldsymbol{\Phi}^{-1}\boldsymbol{S} & \boldsymbol{\Phi}^{-1} & 0\\ \hline \boldsymbol{C}_p & \boldsymbol{C}_p\boldsymbol{\Phi}^{-1}\boldsymbol{S} & \boldsymbol{C}_p\boldsymbol{\Phi}^{-1} & \boldsymbol{C}_p-\boldsymbol{C}_u \end{array}\right]}_{\boldsymbol{G}_{\boldsymbol{e},(\boldsymbol{z}(0),\boldsymbol{w}_u)}}\begin{bmatrix}\hat{\boldsymbol{\eta}}_1\\ \hat{\boldsymbol{\eta}}_2\\ \hline \boldsymbol{z}(0)\\ \hat{\boldsymbol{w}}_u\end{bmatrix} \tag{15}$$

The overall feedback structure wrapped around $\boldsymbol{G}_{\boldsymbol{e},(\boldsymbol{z}(0),\boldsymbol{w}_u)}$ is

$$\begin{bmatrix}\hat{\boldsymbol{\eta}}_1\\ \hat{\boldsymbol{\eta}}_2\\ \hline \boldsymbol{z}(0)\\ \hat{\boldsymbol{w}}_u\end{bmatrix}=\underbrace{\begin{bmatrix}\delta\boldsymbol{I} & 0 & 0\\ 0 & \delta\boldsymbol{I} & 0\\ 0 & 0 & \boldsymbol{\Delta}_f\end{bmatrix}}_{\boldsymbol{\Delta}(\delta,\delta,\boldsymbol{\Delta}_f)}\begin{bmatrix}\hat{\boldsymbol{v}}_1\\ \hat{\boldsymbol{v}}_2\\ \hline \hat{\boldsymbol{e}}\end{bmatrix}, \tag{16}$$

itself defining the structure $\mathcal{D}$. We have the following

Theorem 3: $\|\boldsymbol{T}^u_{\boldsymbol{e},(z(0),\boldsymbol{w}_u)}(s,\delta)\| \leq \mu_{\mathcal{D}}(\boldsymbol{G}_{\boldsymbol{e},(z(0),\boldsymbol{w}_u)}(s))$, for $\delta < 1/\mu_{\mathcal{D}}(\boldsymbol{G}_{\boldsymbol{e},(z(0),\boldsymbol{w}_u)}(s))$ with $\mathcal{D}=\{\boldsymbol{\Delta}(\delta,\delta,\boldsymbol{\Delta}_f)\}$.

D. Effect of initial state preparation error with uncertain C

Finally, we combine the effects of uncertain dynamics, initial state preparation error and uncertain observations, enforcing the structure of Eq. (9) in Eq. (14). As before $\hat{\boldsymbol{\eta}}_1$ is the $\hat{\boldsymbol{z}}$ response to $\hat{\boldsymbol{w}}_u$ and $\hat{\boldsymbol{v}}_2$ the $\hat{\boldsymbol{z}}$ response to $\boldsymbol{z}(0)$. The signal $\hat{\boldsymbol{v}}_2$ needs to be brought to the input, which is done via a copy $\hat{\boldsymbol{v}}_3$ of $\hat{\boldsymbol{v}}_2$ and the feedback $\hat{\boldsymbol{\eta}}_3=\boldsymbol{I}\hat{\boldsymbol{v}}_3$. Now, $\hat{\boldsymbol{\eta}}_3$ is the $\hat{\boldsymbol{z}}$ response to $\boldsymbol{z}(0)$. Substituting $\boldsymbol{C}_u+\delta_c\boldsymbol{S}_c$ for $\boldsymbol{C}_p$ and $\delta_c\boldsymbol{S}_c$ for $\boldsymbol{C}_p-\boldsymbol{C}_u$ reveals the need to generate signals $\delta_c\hat{\boldsymbol{z}}=\delta_c\hat{\boldsymbol{\eta}}_1+\delta_c\hat{\boldsymbol{\eta}}_3$ and $\delta_c\hat{\boldsymbol{w}}_p$ at the input to reconstruct $\hat{\boldsymbol{e}}$. Such signals are easily generated by additional δ_c-feedbacks from a copy $\hat{\boldsymbol{v}}_4$ of $\hat{\boldsymbol{\eta}}_1$, a copy $\hat{\boldsymbol{v}}_5$ of $\hat{\boldsymbol{w}}_u$, a copy $\hat{\boldsymbol{v}}_6$ of $\hat{\boldsymbol{\eta}}_3$ to $\hat{\boldsymbol{\eta}}_4$, $\hat{\boldsymbol{\eta}}_5$, $\hat{\boldsymbol{\eta}}_6$, resp. This yields

$$\begin{bmatrix}\hat{\boldsymbol{v}}_1\\ \hat{\boldsymbol{v}}_2\\ \hline \hat{\boldsymbol{v}}_3\\ \hline \hat{\boldsymbol{v}}_4\\ \hat{\boldsymbol{v}}_5\\ \hat{\boldsymbol{v}}_6\\ \hline \hat{\boldsymbol{e}}\end{bmatrix}=\left[\begin{array}{cccccc|cc} \boldsymbol{X} & 0 & 0 & 0 & 0 & 0 & 0 & \boldsymbol{X}\\ 0 & \boldsymbol{X} & 0 & 0 & 0 & 0 & \boldsymbol{\Phi}^{-1} & 0\\ \hline 0 & \boldsymbol{X} & 0 & 0 & 0 & 0 & \boldsymbol{\Phi}^{-1} & 0\\ \hline \boldsymbol{I} & 0 & 0 & 0 & 0 & 0 & 0 & 0\\ 0 & 0 & 0 & 0 & 0 & 0 & 0 & \boldsymbol{I}\\ 0 & 0 & \boldsymbol{I} & 0 & 0 & 0 & 0 & 0\\ \hline \boldsymbol{C}_u & 0 & \boldsymbol{C}_u & \boldsymbol{S}_c & \boldsymbol{S}_c & \boldsymbol{S}_c & 0 & 0 \end{array}\right]\begin{bmatrix}\hat{\boldsymbol{\eta}}_1\\ \hat{\boldsymbol{\eta}}_2\\ \hline \hat{\boldsymbol{\eta}}_3\\ \hline \hat{\boldsymbol{\eta}}_4\\ \hat{\boldsymbol{\eta}}_5\\ \hat{\boldsymbol{\eta}}_6\\ \hline \boldsymbol{z}(0)\\ \hat{\boldsymbol{w}}_u\end{bmatrix} \tag{17}$$

with $\boldsymbol{X}=\boldsymbol{\Phi}^{-1}\boldsymbol{S}$ and the overall structured perturbation feedback

$$\begin{bmatrix}\hat{\boldsymbol{\eta}}_1\\ \hat{\boldsymbol{\eta}}_2\\ \hline \hat{\boldsymbol{\eta}}_4\\ \hat{\boldsymbol{\eta}}_5\\ \hat{\boldsymbol{\eta}}_6\end{bmatrix}=\left[\begin{array}{cc|ccc} \delta\boldsymbol{I} & 0 & 0 & 0 & 0\\ 0 & \delta\boldsymbol{I} & 0 & 0 & 0\\ \hline 0 & 0 & \delta_c\boldsymbol{I} & 0 & 0\\ 0 & 0 & 0 & \delta_c\boldsymbol{I} & 0\\ 0 & 0 & 0 & 0 & \delta_c\boldsymbol{I} \end{array}\right]\begin{bmatrix}\hat{\boldsymbol{v}}_1\\ \hat{\boldsymbol{v}}_2\\ \hline \hat{\boldsymbol{v}}_4\\ \hat{\boldsymbol{v}}_5\\ \hat{\boldsymbol{v}}_6\end{bmatrix}.$$

The feedback $\hat{\boldsymbol{\eta}}_3=\boldsymbol{I}\hat{\boldsymbol{v}}_3$ is implemented by elimination of $\hat{\boldsymbol{\eta}}_3$, that is, $\hat{\boldsymbol{\eta}}_3=\boldsymbol{\Phi}^{-1}\boldsymbol{S}\hat{\boldsymbol{\eta}}_2+\boldsymbol{\Phi}^{-1}\boldsymbol{z}(0)$. Injecting the latter in the above yields

$$\begin{bmatrix}\hat{\boldsymbol{v}}_1\\ \hat{\boldsymbol{v}}_2\\ \hline \hat{\boldsymbol{v}}_4\\ \hat{\boldsymbol{v}}_5\\ \hat{\boldsymbol{v}}_6\\ \hline \hat{\boldsymbol{e}}\end{bmatrix}=\underbrace{\left[\begin{array}{cccccc|cc} \boldsymbol{X} & 0 & 0 & 0 & 0 & 0 & 0 & \boldsymbol{X}\\ 0 & \boldsymbol{X} & 0 & 0 & 0 & 0 & \boldsymbol{\Phi}^{-1} & 0\\ \hline \boldsymbol{I} & 0 & 0 & 0 & 0 & 0 & 0 & 0\\ 0 & 0 & 0 & 0 & 0 & 0 & 0 & \boldsymbol{I}\\ 0 & \boldsymbol{X} & 0 & 0 & 0 & 0 & \boldsymbol{\Phi}^{-1} & 0\\ \hline \boldsymbol{C}_u & \boldsymbol{C}_u\boldsymbol{X} & \boldsymbol{S}_c & \boldsymbol{S}_c & \boldsymbol{S}_c & \boldsymbol{C}_u\boldsymbol{\Phi}^{-1} & 0 \end{array}\right]}_{\boldsymbol{G}^c_{\boldsymbol{e},(\boldsymbol{z}(0),\boldsymbol{w}_p)}}\begin{bmatrix}\hat{\boldsymbol{\eta}}_1\\ \hat{\boldsymbol{\eta}}_2\\ \hline \hat{\boldsymbol{\eta}}_4\\ \hat{\boldsymbol{\eta}}_5\\ \hat{\boldsymbol{\eta}}_6\\ \hline \boldsymbol{z}(0)\\ \hat{\boldsymbol{w}}_u\end{bmatrix}. \tag{18}$$

with $\boldsymbol{X}=\boldsymbol{\Phi}^{-1}\boldsymbol{S}$ and overall feedback $\boldsymbol{\Delta}(\delta,\delta,\delta_c,\delta_c,\delta_c,\boldsymbol{\Delta}_f)$. The latter feedback that defines the structure $\mathcal{D}$ is not written explicitly as it should by now be obvious from Eqs. (7), (12), (16). Consequently, we get

Theorem 4: Setting $\mathcal{D}=\{\boldsymbol{\Delta}(\delta,\delta,\delta_c,\delta_c,\delta_c,\boldsymbol{\Delta}_f)\}$, we have

$$\|\boldsymbol{T}^u_{\boldsymbol{e},(z(0),\boldsymbol{w}_u)}(s,\delta,\delta_c)\| \leq \mu_{\mathcal{D}}(\boldsymbol{G}^c_{\boldsymbol{e},(z(0),\boldsymbol{w}_u)}(s))$$

for $\delta < 1/\mu_{\mathcal{D}}(\boldsymbol{G}^c_{\boldsymbol{e},(z(0),\boldsymbol{w}_u)}(s))$.

IV. Robust performance in the perturbed formulation

We consider the point of view taken by Eq. (2b) with a *perturbed* driving term $\boldsymbol{w}_p$. Taking its Laplace transform yields

$$(s\boldsymbol{I}-\boldsymbol{A})\hat{\boldsymbol{z}}(s)=\delta\boldsymbol{S}\hat{\boldsymbol{w}}_p(s)+\boldsymbol{z}(0), \tag{19a}$$
$$\hat{\boldsymbol{e}}(s)=\boldsymbol{C}_u\hat{\boldsymbol{z}}(s)+(\boldsymbol{C}_p-\boldsymbol{C}_u)\hat{\boldsymbol{w}}_p(s). \tag{19b}$$

A. Zero initial error

If $s\boldsymbol{I}-\boldsymbol{A}$ is invertible and there is no initial state preparation error, introducing the structured uncertainty $\boldsymbol{C}_p-\boldsymbol{C}_u=\delta_c\boldsymbol{S}_c$ yields

$$\boldsymbol{T}^p_{\boldsymbol{e},\boldsymbol{w}_p}(s,\delta,\delta_c)=\boldsymbol{C}_u\boldsymbol{\Phi}^{-1}(s)\delta\boldsymbol{S}+\delta_c\boldsymbol{S}_c. \tag{20}$$

Bounding $\|\boldsymbol{T}^p_{\boldsymbol{e},\boldsymbol{w}_p}(s,\delta)\|$ can be trivially although conservatively done by

$$\|\boldsymbol{T}^p_{\boldsymbol{e}\boldsymbol{w}_p}(s,\delta,\delta_c)\|\le\|\begin{bmatrix}\boldsymbol{C}_u\boldsymbol{\Phi}^{-1}(s)\boldsymbol{S} & \boldsymbol{S}_c\end{bmatrix}\|\sqrt{\delta^2+\delta_c^2}, \tag{21}$$

without recourse to the robust performance analysis. The perturbed case, hence, offers a new approach, circumventing the structured singular value.

It is, however, of interest to approach the problem in the robust performance context, observing that $\boldsymbol{T}^p_{\boldsymbol{e},\boldsymbol{w}_p}(s,\delta,\delta_c)$ is obtained from

$$\begin{bmatrix}\hat{\boldsymbol{v}}_1\\ \hat{\boldsymbol{v}}_2\\ \hline \hat{\boldsymbol{e}}\end{bmatrix}=\underbrace{\left[\begin{array}{cc|c}0&0&\boldsymbol{I}\\0&0&\boldsymbol{I}\\\hline \boldsymbol{C}_u\boldsymbol{\Phi}^{-1}\boldsymbol{S}&\boldsymbol{S}_c&0\end{array}\right]}_{G^c_{\boldsymbol{e},\boldsymbol{w}_p}}\begin{bmatrix}\hat{\boldsymbol{\eta}}_1\\ \hat{\boldsymbol{\eta}}_2\\ \hline \hat{\boldsymbol{w}}_p\end{bmatrix} \tag{22}$$

after the feedback

$$\begin{bmatrix}\hat{\boldsymbol{\eta}}_1\\ \hat{\boldsymbol{\eta}}_2\end{bmatrix}=\begin{bmatrix}\delta\boldsymbol{I}&0\\0&\delta_c\boldsymbol{I}\end{bmatrix}\begin{bmatrix}\hat{\boldsymbol{v}}_1\\ \hat{\boldsymbol{v}}_2\end{bmatrix}. \tag{23}$$

With $\boldsymbol{\Delta}(\delta,\delta_c,\boldsymbol{\Delta}_f)$ as defining the structure $\mathcal{D}$, we have the following theorem, which differs from the classical robust performance of Th. 1:

Theorem 5: $\|\boldsymbol{T}^p_{\boldsymbol{e},\boldsymbol{w}_p}(j\omega,\delta,\delta_c)\|\le\mu_{\mathcal{D}}(\boldsymbol{G}^c_{\boldsymbol{e},\boldsymbol{w}_p}(j\omega))$, for δ such that $\boldsymbol{w}_p\in L^2$.

Proof: Observe that $\det(\boldsymbol{I}-\boldsymbol{G}^c_{\boldsymbol{e},\boldsymbol{w}_u}(s)\boldsymbol{\Delta})=\det(\boldsymbol{I}-\boldsymbol{T}^p_{\boldsymbol{e},\boldsymbol{w}_u}(s,\delta,\delta_c)\boldsymbol{\Delta}_f)$. Enforcing $\det(\boldsymbol{I}-\boldsymbol{G}^c_{\boldsymbol{e},\boldsymbol{w}_u}(j\omega)\boldsymbol{\Delta})\neq 0$ therefore bounds $\boldsymbol{T}^p_{\boldsymbol{e},\boldsymbol{w}_u}(j\omega,\delta,\delta_c)$ but does not enforce robust stability which is dealt with separately by enforcing $\boldsymbol{w}_p$ to be a square integrable signal. ∎

Observe that the bound of Th. 5 holds for all δ's, but that $\|\boldsymbol{T}^p_{\boldsymbol{e},\boldsymbol{w}_p}(j\omega,\delta,\delta_c)\|_\infty$ is a valid operator norm only for $w_p\in L^2$, hence the restriction on δ.

B. Effect of initial state preparation error

A significant difference between the unperturbed and the perturbed case is that in the latter the effect of $\boldsymbol{z}(0)$ is completely decoupled from $\hat{\boldsymbol{w}}_p$, as seen by the transfer matrix

$$\boldsymbol{T}^p_{\boldsymbol{e},(\boldsymbol{z}(0),\boldsymbol{w}_p)}(s,\delta,\delta_c)=\begin{bmatrix}\boldsymbol{C}_u\boldsymbol{\Phi}^{-1}(s) & \boldsymbol{C}_u\boldsymbol{\Phi}^{-1}(s)\delta\boldsymbol{S}+\delta_c\boldsymbol{S}_c\end{bmatrix}. \tag{24}$$

Bounding $\|\boldsymbol{T}^p_{\boldsymbol{e},(z(0),\boldsymbol{w}_p)}(s,\delta,\delta_c)\|$ is again trivial,

$$\|\boldsymbol{T}^p_{\boldsymbol{e},(\boldsymbol{z}(0),\boldsymbol{w}_p)}(s,\delta,\delta_c)\|\le\|\boldsymbol{C}_u\boldsymbol{\Phi}^{-1}(s)\|+\|\begin{bmatrix}\boldsymbol{C}_u\boldsymbol{\Phi}^{-1}(s)\boldsymbol{S} & \boldsymbol{S}_c\end{bmatrix}\|\sqrt{\delta^2+\delta_c^2}, \tag{25}$$

and does not require the robust performance analysis. It, hence, offers a new approach.

If a robust performance analysis based on structured singular value analysis is desired, it can be accomplished via

$$\begin{bmatrix}\hat{\boldsymbol{v}}_1\\ \hat{\boldsymbol{v}}_2\\ \hline \hat{\boldsymbol{e}}\end{bmatrix}=\underbrace{\left[\begin{array}{cc|c}0&0&\boldsymbol{I}\\0&0&\boldsymbol{I}\\\hline \boldsymbol{C}_u\boldsymbol{\Phi}^{-1}\boldsymbol{S}&\boldsymbol{S}_c&\boldsymbol{C}_u\boldsymbol{\Phi}^{-1}\end{array}\right]}_{G^c_{\boldsymbol{e},(\boldsymbol{z}(0),\boldsymbol{w}_p)}}\begin{bmatrix}\hat{\boldsymbol{\eta}}_1\\ \hat{\boldsymbol{\eta}}_2\\ \hline \boldsymbol{z}(0)\\ \hat{\boldsymbol{w}}_p\end{bmatrix} \tag{26}$$

after the same feedback as Eq. (23). With the $\mathcal{D}$ structure defined by $\boldsymbol{\Delta}(\delta,\delta_c,\boldsymbol{\Delta}_f)$, we have

Theorem 6: $\|\boldsymbol{T}^p_{\boldsymbol{e},(z(0),\boldsymbol{w}_u)}(s,\delta,\delta_c)\|\le\mu_{\mathcal{D}}(\boldsymbol{G}^c_{\boldsymbol{e},(z(0),\hat{\boldsymbol{w}}_u)}(s))$ for $s=j\omega$ and δ such that $\boldsymbol{w}_p\in L^2$.

V. Benchmark Mechanical Example: Double Spring-Mass-Dashpot

To illustrate the perturbed vs. unperturbed approach, we consider a simple system that has been a benchmark problem for robust control synthesis [24]: the double spring-mass-dashpot system of [25, Example 4.2], where n_1, n_2 are the forces acting on masses m_1, m_2, resp., and e_1, e_2 are the rates of motion of masses m_1, m_2, resp., relative to the spring rest positions:

$$\frac{d}{dt}\boldsymbol{r}_u=\begin{bmatrix}\boldsymbol{Z}&\boldsymbol{I}\\ \boldsymbol{M}_1&\boldsymbol{M}_2\end{bmatrix}\boldsymbol{r}_u+\begin{bmatrix}\boldsymbol{Z}\\ \boldsymbol{I}\end{bmatrix}\boldsymbol{n}, \tag{27a}$$
$$\boldsymbol{e}=\left[\begin{array}{cc|cc}0&0&m_1^{-1}&0\\0&0&0&m_2^{-1}\end{array}\right]\boldsymbol{r}_u, \tag{27b}$$

where $\boldsymbol{Z}=\begin{bmatrix}0&0\\0&0\end{bmatrix}$, $\boldsymbol{I}=\begin{bmatrix}1&0\\0&1\end{bmatrix}$ is the identity matrix, and

$$\boldsymbol{M}_1=\begin{bmatrix}-\frac{k_1}{m_1}&\frac{k_1}{m_2}\\ \frac{k_1}{m_1}&-\frac{k_1+k_2}{m_2}\end{bmatrix},\quad \boldsymbol{M}_2=\begin{bmatrix}-\frac{b_1}{m_1}&\frac{b_1}{m_2}\\ \frac{b_1}{m_1}&-\frac{b_1+b_2}{m_2}\end{bmatrix}.$$

$k_1,k_2>0$ and $b_1,b_2>0$ are the stiffness and damping constants of the springs, where the first spring connects m_1 to a fixed point and the second spring connects m_1 to m_2. As m_1 and m_2 appear in both $\boldsymbol{A}$ and $\boldsymbol{C}$, if the masses are uncertain, a minor modification of the method of Sec. III-B is needed, as explained in Remark 3.

In this case-study, $\boldsymbol{T}_{\boldsymbol{e},\boldsymbol{n}}$ is a mapping from force actuators to *co-located* rate sensors, well known to be *passive*, *dissipative* or *positive real* [11], [15]. Here, co-location means that the force n_i applies to the mass m_i and that e_i measures the rate of motion of m_i. Passive means that, for $\boldsymbol{r}_u(0)=0$, there exists a constant $\epsilon>0$ such that $\int_0^T\boldsymbol{e}^T(t)\boldsymbol{n}(t)\,dt>\epsilon\|\boldsymbol{n}\|^2_{L^2[0,T]}$, $\forall T>0,\forall\boldsymbol{n}\in L^2[0,T]$. For such a system, any feedback $\boldsymbol{n}=-D\boldsymbol{e}=-DC\boldsymbol{r}_u$, where $D=D^T>0$, preserves closed-loop stability, similar to a bias-field-mediated feedback in quantum spintronic systems, which also preserves stability [7].

This "positive real" design [11], [15] has been widely applied to space structures with the caveat that for distributed parameter systems with vibration eigenfrequencies $\omega_{k\to\infty}\to\infty$, it is difficult to maintain co-location of the sensors and actuators. Indeed, if ε is the distance between the actuating and the sensing points, there exists a k such that $\varepsilon\in[\lambda_k/2,\lambda_k]$,

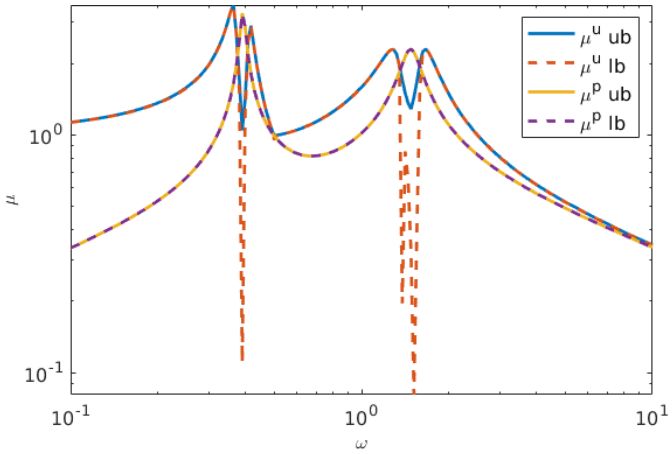

(a) Uncertain stiffness k_1

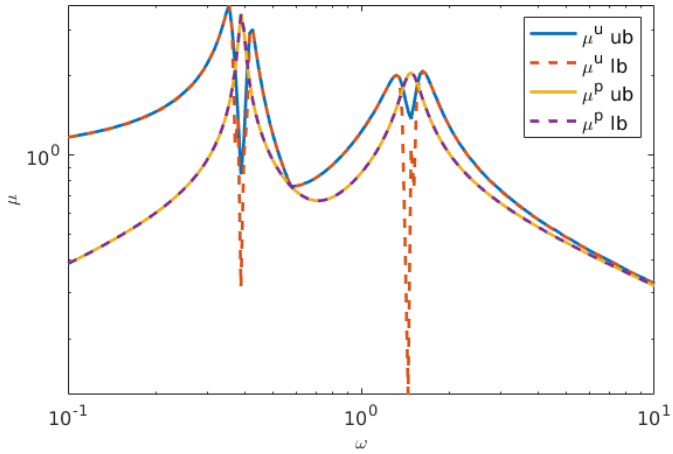

(b) Uncertain stiffness k_2

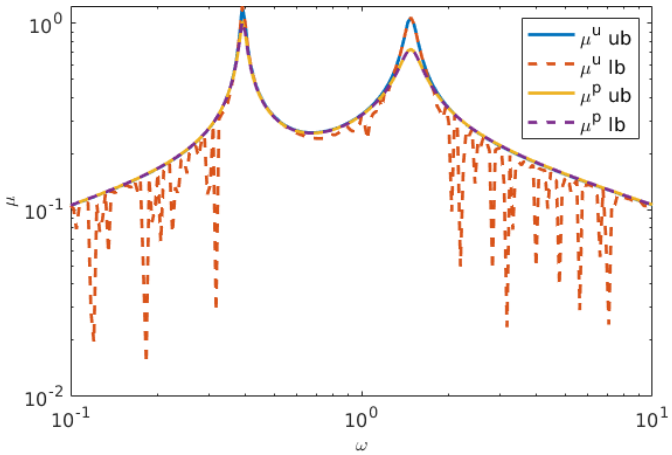

(c) Uncertain damping b_1

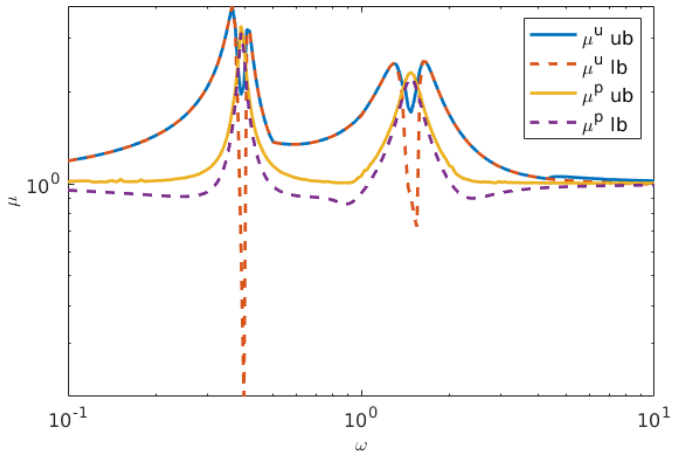

(d) Stiffness k_1 uncertainty and sensor-actuator misalignment (S_c)

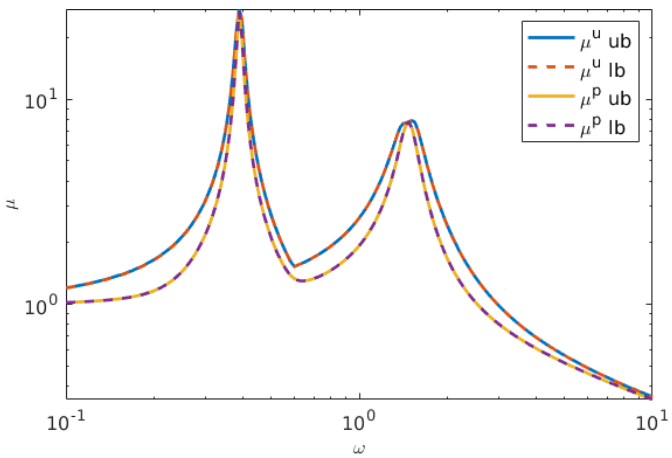

(e) Combination of stiffness k_1 uncertainty and initial error $\boldsymbol{z}(0)$

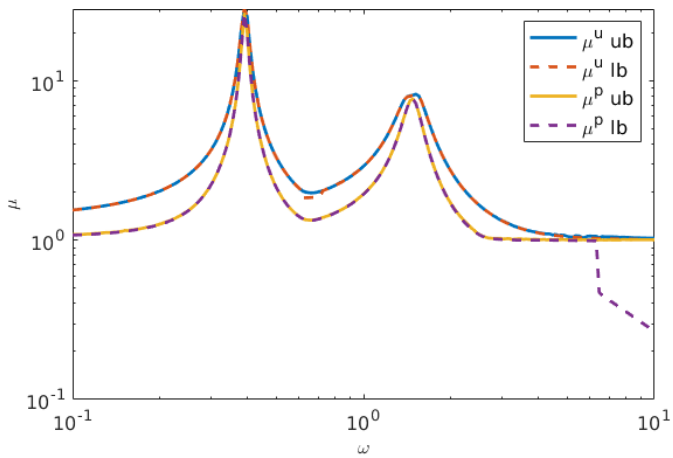

(f) Stiffness k_1 uncertainty, initial error $\boldsymbol{z}(0)$ and S_c uncertainty C

Fig. 1: Upper and lower bounds on the structured singular value μ for unperturbed and perturbed formulations for different combinations of uncertainties for the spring-mass dashpot system with $m_1 = 3, m_2 = 1$, $k_1 = k_2 = 1$, $b_1 = b_2 = 0.1$.

where $\lambda_k = 2\pi c/\omega_k$ is the wavelength of the vibration mode ω_k and c is the propagation speed of the elastic disruption. In this situation, the feedback from the sensing point to the actuating point is no longer negative, but positive. Hence, it destabilizes the vibration mode ω_k. In the present setup of Eq. (27), a co-location error could be modeled as the structured perturbation

$$\boldsymbol{S}_c = \left[\begin{array}{cc|cc} 0 & 0 & 0 & m_2^{-1} \\ 0 & 0 & m_1^{-1} & 0 \end{array}\right], \tag{28}$$

meaning that e_1 blends the rates of motion of m_1 and m_2.

Positive realness also has a circuit theory formulation, where $\boldsymbol{n}$ is the voltage and $\boldsymbol{e}$ the current of a passive n-port [1]. Such circuit models have been used to simulate quantum phenomena [4], in particular four-dimensional topological insulators [23]. Co-location in this context means that the voltage is measured at the same port at which the current is injected.

A. Uncertain stiffness or damping

We first consider a relative uncertainty in the stiffness k_1 modeled as $k_1(1+\delta)$. The unperturbed μ^u is computed using Th. 1; the perturbed μ^p is computed using Th. 5 after removal of the second row and column of $\boldsymbol{G}^c_{\boldsymbol{e},\boldsymbol{w}_p}$ as defined by Eq. (22), as $\delta_c = 0$. The results, illustrated in Fig. 1a, reveal two regimes: $\mu^p(\jmath\omega) > \mu^u(\jmath\omega)$ around the resonant frequencies and the reverse inequality $\mu^p(\jmath\omega) < \mu^u(\jmath\omega)$ away from the resonances. To explain this phenomenon, consider

$$\begin{aligned} \det(\boldsymbol{I} - \boldsymbol{G}^u\boldsymbol{\Delta}) &= \det(\boldsymbol{I} - \Phi^{-1}\delta\boldsymbol{S})\times \\ &\qquad \det(\boldsymbol{I} - \boldsymbol{T}^p(I - \Phi^{-1}\delta S)^{-1}\boldsymbol{\Delta}_f), \quad (29a) \\ \det(\boldsymbol{I} - \boldsymbol{G}^p\boldsymbol{\Delta}) &= \det(\boldsymbol{I} - \boldsymbol{T}^p\boldsymbol{\Delta}_f), \quad (29b) \end{aligned}$$

which is obtained by direct matrix manipulations and replacing $\boldsymbol{T}^u$ by its expression derived from Eq. (5). At the exact unperturbed resonance, $\|\boldsymbol{T}^p\|$ reaches its maximum, while $\boldsymbol{T}^u = \boldsymbol{T}^p(\boldsymbol{I} - \boldsymbol{\Phi}^{-1}\delta\boldsymbol{S})^{-1}$ is damped by $(\boldsymbol{I} - \boldsymbol{\Phi}^{-1}\delta\boldsymbol{S})^{-1}$ since $\boldsymbol{\Phi}^{-1}$ also achieves its maximum at the resonant eigefrequencies. Therefore, at exact resonance, $\|\boldsymbol{T}^u\| < \|\boldsymbol{T}^p\|$. Denoting by $\boldsymbol{\Delta}^u_f$, $\boldsymbol{\Delta}^p_f$ the $\boldsymbol{\Delta}_f$, for which the determinant in Eq. (29a) and Eq. (29b), resp., vanishes, we have $\|\boldsymbol{\Delta}^u_f\| > \|\boldsymbol{\Delta}^p_f\|$, while $|\delta|$, the relative error on the stiffness, is bounded by 1 to preserve closed-loop stability. Hence $\mu^u = 1/\|\boldsymbol{\Delta}^u_f\| < \mu^p = 1/\|\boldsymbol{\Delta}^p_f\|$, as shown by Figs. 1a, 1b at the exact resonant frequency. Away from both the exact and the perturbed resonances, and under the assumption that both $\|\boldsymbol{T}^u\|$ and $\|\boldsymbol{T}^p\|$ are sufficiently damped (precisely < 1), δ becomes the deciding factor of μ in the sense that $\mu^u = 1/\min_{\boldsymbol{\Delta}} \max\{\|\boldsymbol{\Delta}_f\|, |\delta|\} = |\delta| = 1$ for the unperturbed case. For the perturbed case, since δ is not involved in stability, $\mu^p = 1/\min_{\boldsymbol{\Delta}} \max\{\|\boldsymbol{\Delta}_f\|, |\delta|\} = \|\boldsymbol{T}^p\| < 1$. Hence, under sufficient damping far from the resonance, $\mu^u > \mu^p$, again shown by Figs. 1a, 1b.

With regard to the damping parameters, the linear damping model is an approximation of an essentially nonlinear stress-strain hysteresis in the spring material. The results of uncertain damping $b_1(1+\delta)$ for the same numerical example in Eq. (27) using Theorems 1, 5 are shown in Fig. 1c. Observe that the upper bounds on the unperturbed and perturbed μ reach their maxima at the same frequency $\bar{\mu}^p(0.79) = \bar{\mu}^u(0.79) = 0.65$ and $\bar{\mu}^p(2.2) = \bar{\mu}^u(2.2) = 1.3$. This is not surprising, as uncertainty in the damping does not change the resonant frequency.

	ω	$\mu^p(i\omega)$	$\delta_{\max}(s) = \mu^{-1}(s)$	$\|\boldsymbol{T}^p(s, \delta_{\max}, 0)\|$
S_1	0.389	3.2502	0.3077	3.2502
	1.4791	2.2981	0.4351	2.2981
S_2	0.389	3.4448	0.2903	3.4448
	1.4791	2.0611	0.4852	2.0611
S_3	0.389	1.0278	0.973	1.0278
	1.4791	0.7267	1.276	0.7267
S_4	0.3890	1.0893	0.918	1.0893
	1.4791	0.6518	1.5340	0.6518

TABLE I: Comparison of $\mu(s)$ for the perturbed case vs $\|\boldsymbol{T}^p_{\boldsymbol{e},(\boldsymbol{z}(0),\boldsymbol{w}_p)}(s, \delta, \delta_c)\|$ calculated according to Eq. (25) with $\delta = \mu(s)^{-1}$, $\delta_c = 0$, $s = i\omega$ for structured perturbations S_1 to S_4 corresponding to perturbation of the stiffness constants k_1, k_2 and damping rates b_1, b_2, respectively.

B. Sensor-actuator misalignment and initial state errors

In the presence of sensor mis-alignment, μ is computed by appealing to Th. 2, Eq. (11) in the unperturbed case, and Th. 5, Eq. (22) in the perturbed case. The results are shown in Fig. 1d. As before the unperturbed and perturbed cases yield close results at the resonant frequencies that, here, are shifted relative to the stiffness k_1 uncertainty case.

Keeping k_1 uncertain but adding an initial state error $\boldsymbol{z}(0)$ instead of a collocation error, as in Th. 3 of Sec. III-C for the unperturbed case and Th. 6 of Sec. IV-B for the perturbed case, the unperturbed μ is computed from Eq. (15) after setting $\boldsymbol{C}_p = \boldsymbol{C}$ and $\boldsymbol{C}_p - \boldsymbol{C}_u = 0$. The perturbed μ is computed from Eq. (26), after removal of the second row and second column of $\boldsymbol{G}^c_{\boldsymbol{e},(\boldsymbol{z}(0),\boldsymbol{w}_p)}$. The results in Fig. 1e show again consistency between the unperturbed and perturbed cases. It is also worth noting that the μ has increased compared with the simplest case of k_1 uncertainty, as a result of the initial state error.

The combined effect of uncertainties in k_1, $z(0)$ and $\boldsymbol{S}_c$ (for the same model system) are shown in Fig. 1f. The unperturbed case is dealt with by Th. 4 and the perturbed case by Th. 6.

C. Comparison of μ and direct bounds

In the perturbed case Eq. (25) provides explicit bounds on the norm of the transfer function, which we can compare to the bounds obtained from μ-analysis. Table I shows that the explicit bounds on $\|\boldsymbol{T}^p_{\boldsymbol{e},(\boldsymbol{z}(0),\boldsymbol{w}_p)}(s, \delta, \delta_c)\|$ for $\delta = 1/\mu^p$ in the absence of initial state and co-location errors are in excellent agreement with the upper bounds obtained for μ^p for different structured perturbations.

VI. Application to Controlling Quantum Systems

Another enlightening application is control of quantum systems. Coherent quantum systems are open-loop purely oscillatory, and neither coherent open-loop controls nor physically relevant structured uncertainties like J-coupling errors can change the closed-loop oscillatory situation [6], [7]. For open quantum systems, decoherence acts as a stabilizing

controller [18], but there are still challenges in applying conventional structured singular value analysis. For example, constants of motion, such as the unit-trace constraint for density operators describing quantum states, create a pole at 0 in $\mathbf{\Phi}^{-1}(s)$ in the real Bloch representation of the dynamics commonly used to describe open quantum systems. However, as noted in Sec II, since the unperturbed error dynamics is driven by the unperturbed dynamics, the frequency sweep could be limited to the resonant frequencies of $\boldsymbol{A}$, which are by definition nonvanishing; hence the (possibly multiple) closed-loop pole at 0 is avoided. The perturbed formulation is theoretically more challenging, since the frequency sweep should include the uncertain resonant frequencies of $\boldsymbol{A}+\delta\boldsymbol{S}$, and passing over $\omega = 0$ cannot be ruled out. If, while numerically exploring $\mu_{\mathcal{D}}(\omega \to 0)$, it appears that the maximum could be at $\omega = 0$, with the difficulty that $\mathbf{\Phi}^{-1}(0)$ fails to exist, then the formal procedure developed in [20] should be followed. Essentially, $\mathbf{\Phi}^{-1}(s)$ should be replaced by $\mathbf{\Phi}^{\#}(s)$, where $\#$ denotes a specialized pseudo-inverse close in spirit to, but different from, the Moore-Penrose pseudo-inverse. This specialized pseudo-inverse applied to the construction of $\mu_{\mathcal{D}}$ cures the lack of continuity at $s = 0$ and moreover for $s \neq 0$ coincides with the $\mu_{\mathcal{D}}$ derived from $\mathbf{\Phi}^{-1}(s)$. Note that in [10], this case has been approached heuristically by damping the closed-loop systems as $\boldsymbol{A} - \epsilon\boldsymbol{I}$ and then allowing $\epsilon \downarrow 0$.

A. Bias field control of coupled qubit Rabi oscillations

As a concrete example, consider a simple system of two qubits under XX-coupling of strength J, restricted to the single excitation subspace spanned by the states $|L\rangle = |\uparrow\downarrow\rangle$ and $|R\rangle = |\downarrow\uparrow\rangle$, which correspond to excitation of the left and right qubit, respectively. It is instructive to consider the two-qubit problem, which is analytically solvable, but the model can be extended to chains of more than two qubits and more complex networks. While the latter networks are generally not amenable to analytic solutions, numerical optimization suggests that high fidelities and good transfer times can be achieved by non-zero optimal biases, and that transfer fidelities may be robust to uncertainties in system parameters under certain conditions [8], [17].

B. Dynamics

For two qubits the coherent dynamics in the single-excitation subspace can be modeled by the Hamiltonian

$$H = \hbar \begin{bmatrix} D_1 & J \\ J & D_2 \end{bmatrix},$$

where $\hbar$ is the reduced Planck constant and $\hbar J$ and $\hbar D_k$ are exchange coupling and onsite potential energies, respectively. We assume that the local onsite potentials can be controlled via local electric or magnetic fields that shift the energy levels of the qubit, e.g., via Stark or Zeeman shifts, respectively, i.e., D_1 and D_2 serve as controls. To include decoherence, the state of the system is described by the density operator ρ, a Hermitian operator with $\mathrm{Tr}(\rho) = 1$, which evolves as

$$\tfrac{d}{dt}\rho = -\tfrac{\imath}{\hbar}[H,\rho] + \gamma\mathfrak{L}[V]\rho, \tag{30}$$

where $\mathfrak{L}[V]$ is a typical Lindbladian,

$$\mathfrak{L}[V]\rho = V\rho V^\dagger - \tfrac{1}{2}(V^\dagger V\rho + \rho V^\dagger V). \tag{31}$$

To model typical decoherence, which acts as dephasing in the Hamiltonian basis, we choose V to be a Hermitian operator that commutes with the Hamiltonian, $[H,V] = 0$. We take

$$V = \frac{1}{2J_{\text{eff}}}\begin{bmatrix} -\Delta & 2J \\ 2J & \Delta \end{bmatrix}.$$

where $\Delta := D_2 - D_1$ is the detuning and $J_{\text{eff}} = \sqrt{\Delta^2 + 4J^2}$. Δ/J is dimensionless, $\hbar\Delta$ is the difference between the energy levels of the left and right qubit and γ is the decoherence rate.

The dynamics can be reformulated in a way similar to the state space formulation classically used in robustness analysis using the Bloch equation formulation [5], [14], [21], [22], here rewritten in line with Eqs. (1a) and (1b),

$$\tfrac{d}{dt}\boldsymbol{r}_u = \underbrace{(\boldsymbol{A}_H + \boldsymbol{A}_{\mathfrak{L}})}_{\boldsymbol{A}}\boldsymbol{r}_u + \boldsymbol{B}\boldsymbol{n}, \tag{32a}$$

$$\tfrac{d}{dt}\boldsymbol{r}_p = \underbrace{(\boldsymbol{A}_H + \boldsymbol{A}_{\mathfrak{L}} + \delta\boldsymbol{S})}_{\boldsymbol{A}+\delta\boldsymbol{S}}\boldsymbol{r}_u + \boldsymbol{B}\boldsymbol{n}. \tag{32b}$$

This formulation is obtained by expanding the density operator for the quantum state in terms of the Pauli matrices

$$\sigma_x = \begin{bmatrix} 0 & 1 \\ 1 & 0 \end{bmatrix}, \sigma_y = \begin{bmatrix} 0 & -i \\ i & 0 \end{bmatrix}, \sigma_z = \begin{bmatrix} 1 & 0 \\ 0 & -1 \end{bmatrix}, I = \begin{bmatrix} 1 & 0 \\ 0 & 1 \end{bmatrix}. \tag{33}$$

For a two-qubit system it is customary to use the expansion

$$\rho = \tfrac{1}{2}(r_1\sigma_x + r_2\sigma_y + r_3\sigma_z + I) \tag{34}$$

with regard to the unnormalized Pauli matrices rather than an orthonormal basis for the Hermitian operator on the Hilbert space as this ensures that pure states, characterized by $\mathrm{Tr}(\rho^2) = 1$, are mapped to points $[r_1, r_2, r_3]^T$ on the unit sphere in $\mathbb{R}^3$. Due to trace conservation, the coefficient r_4 is constant, and, with our choice of basis, $r_4 = 1$. Therefore, it makes sense to define the reduced state vector $\boldsymbol{r}_u = [r_1, r_2, r_3]^T \in \mathbb{R}^3$. It can be shown by direct calculation that the corresponding dynamical generators are explicitly

$$\boldsymbol{A}_H = \begin{bmatrix} 0 & \Delta & 0 \\ -\Delta & 0 & -2J \\ 0 & 2J & 0 \end{bmatrix}, \boldsymbol{A}_{\mathfrak{L}} = \frac{-\gamma}{J_{\text{eff}}^2}\begin{bmatrix} \Delta^2 & 0 & 2\Delta J \\ 0 & J_{\text{eff}}^2 & 0 \\ 2\Delta J & 0 & 4J^2 \end{bmatrix}.$$

The matrix $\boldsymbol{A}$ has rank 2 with a pole at 0 for any Δ, J and γ. The oscillatory eigenvalues are $\lambda(\boldsymbol{A}_H + \boldsymbol{A}_{\mathfrak{L}}) = -\gamma \pm \imath J_{\text{eff}}$. This *structural stability* of the eigenvalues obviates the need to consider possible change of multiplicities, as considered in [20].

The excitation in the coupled qubit system undergoes coherent oscillations between the left and right qubit, $\rho_L = |L\rangle\langle L|$ and $\rho_R = |R\rangle\langle R|$, corresponding to $\boldsymbol{r}_L = [0,0,1]^T$ and $\boldsymbol{r}_R = [0,0,-1]^T$, for the unperturbed and perturbed cases. Starting with an excitation of the left qubit, $\rho(0) = \rho_L$, we measure the excitation transfer to the right qubit as a function of time by the overlap $\mathcal{F}_{u,p}(t) = \mathrm{Tr}[\rho_R\rho_{u,p}(t)]$, where $\rho_{u,p}$ denotes the unperturbed or perturbed density [9]. For J, Δ and γ fixed and no noise (and the affine term can be shown to be zero), the evolution is given by $\boldsymbol{r}_u(t) = \exp(t\boldsymbol{A})\boldsymbol{r}_u(0)$, where exp denotes

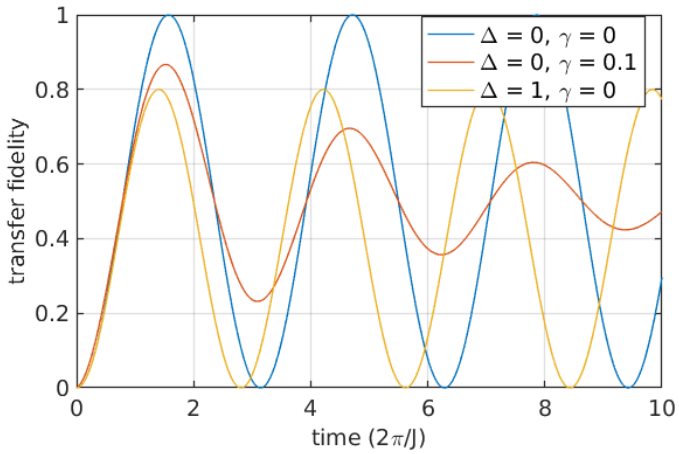

(a) Transfer fidelity oscillations

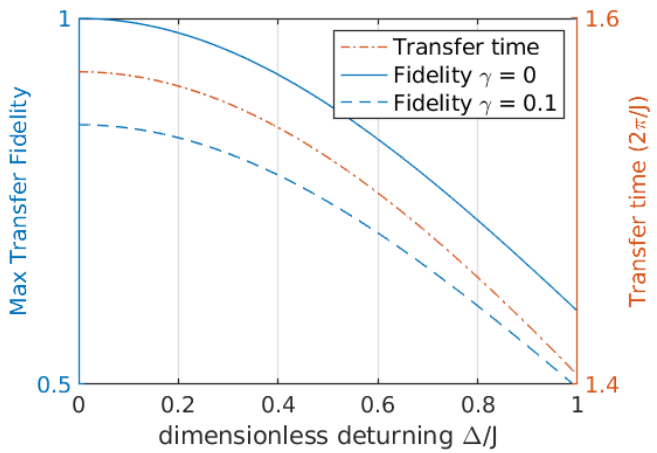

(b) Transfer fidelity and time vs detuning

Fig. 2: Transfer fidelity vs. time and maximum transfer fidelity and minimum transfer time as a function of detuning $\boldsymbol{\Delta}$ for quantum example.

the matrix exponential. Setting $\boldsymbol{r}_{u,p}(t) = (x(t), y(t), z(t))^T_{u,p}$, this shows that $\mathcal{F}_{u,p}(t) = \frac{1}{2}[1 + \boldsymbol{r}_R^T \boldsymbol{r}_{u,p}(t)] = \frac{1}{2}[1 - z_{u,p}(t)]$, and we can explicitly evaluate the matrix exponential to obtain an analytic formula for the transfer fidelity in the unperturbed case,

$$\mathcal{F}_u(t) = \frac{2J^2}{J_{\text{eff}}^2}\left[1 - e^{-t\gamma}\cos(J_{\text{eff}}t)\right]. \tag{35}$$

Eq. (35) shows that the fidelity undergoes damped oscillations as illustrated in Fig. 2(a). The first maximum is achieved for $\cos(J_{\text{eff}}t) = -1$, i.e., a transfer time $t_f = \pi/J_{\text{eff}}$. The corresponding fidelity is

$$\mathcal{F}_u(t_f) = \frac{2J^2}{J_{\text{eff}}^2}[1 + e^{-t_f\gamma}]. \tag{36}$$

Considering $\gamma \geq 0$, the maximum fidelity is $\mathcal{F}_{u,\max}(t_f) = \frac{4J^2}{J_{\text{eff}}^2}$, achieved for $\gamma = 0$. Recalling the definition for $J_{\text{eff}} = \sqrt{\Delta^2 + 4J^2}$, we further see that the absolute maximum of 1 is achieved for $\Delta = 0$ and $J_{\text{eff}} = 2J$. There is a trade-off between the maximum transfer fidelity and the transfer time, however, as $t_f = \pi/J_{\text{eff}}$ implies that the transfer time decreases with increasing Δ. This offers some advantage in terms of increased transfer fidelity, as illustrated in Fig. 2(b), which shows that both the total fidelity and minimal transfer time decrease with increasing detuning Δ. In most practical cases, however, when full state transfer is desired, the speedup due to nonzero Δ is minor compared to the fidelity loss. Additionally, while the fidelity starts at a lower value when decoherence is present, in this case it decreases more slowly with increasing detuning due to the decreased transfer time.

C. Classical structured singular value analysis

The dynamical generator depends on three core parameters Δ, J, and γ, which are often not known precisely. To assess the robustness of observed fidelity oscillations with regard to these parameter uncertainties, we can define structured perturbations. The dependence on γ is linear and thus directly amenable to structured singular value analysis. In what follows, we reserve the symbol δ for general perturbations, and $\delta_{(\ell)}$ with the subscript in parentheses for perturbations on the parameter $\ell = \Delta, \gamma, J$.

The infidelity, either unperturbed or perturbed, is defined as $1 - \mathcal{F}_{u,p}(t) = \frac{1}{2}[1 + z_{u,p}(t)] = \frac{1}{2}[0, 0, 1]\boldsymbol{r}_{u,p} + \frac{1}{2}$, which requires an unusual affine term. The infidelity error, on the other hand, defined as

$$\boldsymbol{e} = (1 - \mathcal{F}_p) - (1 - \mathcal{F}_u) = \mathcal{F}_u - \mathcal{F}_p = \boldsymbol{C}_u \boldsymbol{z}$$

with $\boldsymbol{C}_u = \frac{1}{2}[0, 0, 1]$ and $\boldsymbol{z} = \boldsymbol{r}_p - \boldsymbol{r}_u$, does not require the affine term. Consistently with Eqs. (2a) and (2b), the infidelity error $\boldsymbol{e}$ has two formulations: unperturbed and perturbed.

Considering an uncertainty $\gamma(1 + \delta_{(\gamma)})$ on the decoherence rate, the structure of the perturbation is $\boldsymbol{S} = \gamma \boldsymbol{A}_{\mathfrak{L}}$. Numerical results for $\Delta = 0$, $J = 1$ and $\gamma = 0.01$, shown in Fig. 3 suggest good coincidence between the unperturbed and perturbed analyses but there are differences. In the unperturbed case the graph suggests $\mu^u_\infty = 1.276 > 1$; hence, $\|\boldsymbol{T}^u\|_\infty < 1.272$ for $|\delta| < 1/1.276 = 0.78 < 1$. The restriction $|\delta| < 1$ is consistent with $\gamma_p = \gamma(1+\delta) > 0$, that is, positive perturbed decoherence rate, and hence robust closed-loop stability. Closer inspection of the upper bound for μ^p suggests $\|\boldsymbol{T}^p\|_\infty \leq \mu^p_\infty \approx 0.5946 < 1$ for $\omega = 2$. This bound is tighter than μ^u, but as already noted μ^p does not secure closed-loop stability so that the bound $\|\boldsymbol{T}^p\|_\infty \leq 0.5946$ is only valid for $|\delta| < 1$.

D. Beyond structured singular value: fixed-point iteration

The dependence of $\boldsymbol{A}$ on Δ and J is nonlinear, which poses a challenge for structured singular value analysis. This illustrates its limitations and why new tools are needed, especially for quantum control problems, where parameters typically enter in a nonlinear fashion in the Bloch $\boldsymbol{A}$-matrix. In [19], a fixed-point approach is proposed in lieu of the structured singular value. In essence the perturbation is unstructured and written as $\boldsymbol{A}_p(\delta) - \boldsymbol{A}$ rather than $\boldsymbol{S}\delta$ as in Eqs. (1a)–(1b). In the unperturbed formulation case, $\|\boldsymbol{T}^u_{\boldsymbol{e},\boldsymbol{w}_u}(\delta)\|_\infty \leq \mu$,

$\forall \delta < 1/\mu$, where the strict inequality is required to enforce strict closed-loop stability. Interchanging the role of μ and δ yields $\|\boldsymbol{T}^u_{\boldsymbol{e},\boldsymbol{w}_u}(\delta)\|_\infty < 1/\delta$, leading to the tightening of the inequality by defining

$$\delta_{\max} = \sup\left\{\delta \geq 0 : \|\boldsymbol{T}^u_{\boldsymbol{e},\boldsymbol{w}_u}(\delta)\|_\infty < 1/\delta\right\}. \qquad (37)$$

Whether the *equality* $\|\boldsymbol{T}^u_{\boldsymbol{e},\boldsymbol{w}_u}(\delta_{\max})\|_\infty = 1/\delta_{\max}$ could be achieved depends on whether the limiting factor is closed-loop stability or the transmission norm. In quantum problems as those considered here, the uncertain parameters do not affect stability, and hence the limiting factor is the transmission norm. In such cases, *equality* prevails, and $\delta_{\max}$ is a fixed point of $\delta \mapsto 1/\|\boldsymbol{T}^u_{\boldsymbol{e},\boldsymbol{w}_u}(\delta)\|_\infty$. Note that for the solution to Eq. (37) to be a fixed point, the reverse inequality $\|\boldsymbol{T}^u_{\boldsymbol{e},\boldsymbol{w}_u}(\delta)\|_\infty > 1/\delta$ must hold $\forall \delta > \delta_{\max}$. If there are many such fixed points, the minimum one should be selected. Note that this approach identifies the positive bound; the negative bound $\delta_{\min} < 0$ can be identified in a similar way via the fixed point of $\delta \mapsto -1/\|\boldsymbol{T}^u_{\boldsymbol{e},\boldsymbol{w}_u}(\delta)\|_\infty$.

In the unperturbed and perturbed cases, the fixed point can be computed by graphing $\|\boldsymbol{T}^u_{\boldsymbol{e},\boldsymbol{w}_u}(\delta)\|_\infty$ and $1/\delta$ vs. δ and locating the intersection point of the two plots. More formally, under some circumstances, the contraction mapping theorem can be invoked leading to convergence of the recursion $\delta_{k+1} = 1/\|\boldsymbol{T}^u_{\boldsymbol{e},\boldsymbol{w}_u}(\delta_k)\|_\infty$ to the fixed point. Contraction mapping requires existence of a contraction ratio $\zeta \in (0,1)$ such that

$$|\delta_{k+2} - \delta_{k+1}| < \zeta |\delta_{k+1} - \delta_k|.$$

That is, simplifying the notation to avoid the clutter,

$$\left| \frac{1}{\left\| T\left(\frac{1}{\|T(\delta)\|}\right)\right\|} - \frac{1}{\|T(\delta)\|} \right| < \zeta \left| \frac{1}{\|T(\delta)\|} - \delta \right|.$$

From there, it is easily verified that, for $m > n$,

$$|\delta_m - \delta_n| < \frac{\zeta^m - \zeta^{n-1}}{\zeta - 1} |\delta_1 - \delta_0|.$$

In other words, $\{\delta_k\}_{k=0}^\infty$ is a Cauchy sequence and, hence, converges.

1) Decoherence rate uncertainty: Since the case of an uncertain decoherence rate γ is the only one where the uncertain parameter enters linearly into the Bloch equation and can be safely computed with classical μ, we will use that case as yardstick to gauge how well the fixed point approach works. Taking $\Delta = 0$, $J = 1$, and $\gamma = 0.01$ as before yields $\mu^u = 0.277$ at $\delta_{\max} = 3.6$ and $\mu^u = 1.282$ at $\delta_{\min} = -0.78$ as shown in Fig. 6(c), consistent with the upper bound for μ^u_∞ obtained from the conventional μ-analysis and Fig. 3.

2) Detuning and J-coupling uncertainty: The advantage of the fixed-point iteration approach is that it can applied to assess the effect of uncertainty in the detuning Δ or J-coupling although these parameters appear non-linearly in the dynamics. Figs. 4 and 5 show the perturbed and unperturbed transfer functions and μ for uncertainty in Δ and J, respectively, expanded around $(\Delta, J, \gamma) = (0, 1, 0.01)$. Although there are differences between the transfer functions relative to the unperturbed and perturbed state, both transfer functions have almost the same norm for a wide range of δ and give the same $\delta_{\min}$ and $\delta_{\max}$, as illustrated in Table II. However, the critical frequencies of $\boldsymbol{T}^u$ and $\boldsymbol{T}^p$ are different, especially for perturbation of J, as expected. Comparing the μ plots suggests that $\mu_\infty = \delta_{\max}^{-1}$ is larger for J-coupling uncertainty, which suggests that the system is more sensitive to perturbation of J than Δ. The μ_∞ values for uncertainty in Δ and J are also much larger than μ_∞ for γ uncertainty, suggesting that the system is far less affected by uncertainty in the decoherence rates. In practice, this analysis is useful for understanding where the fundamental limitations of real systems lie and where extra care must be placed when designing a quantum system.

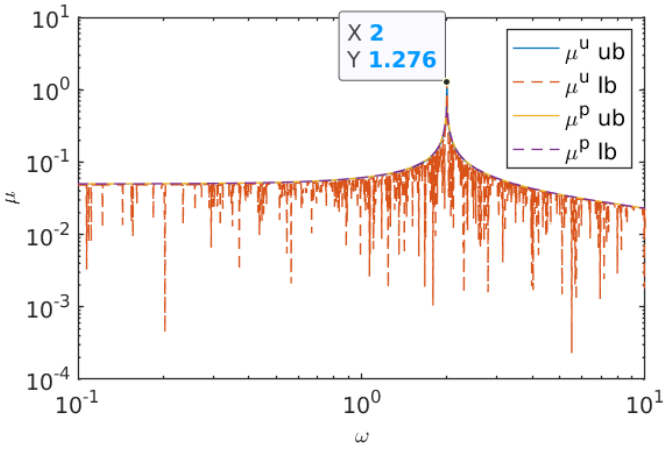

Fig. 3: Upper (ub) and lower (lb) bounds on unperturbed and perturbed μ's for two qubits under decoherence rate uncertainty (system parameters $\Delta = 0$, $J = 1$, $\gamma = 0.01$).

	$\Delta = \Delta_0 + \delta_{(\Delta)}$		$J = J_0 + \delta_{(J)}$		$\gamma = \gamma_0(1 + \delta_{(\gamma)})$	
	$\delta_{\min}$	$\delta_{\max}$	$\delta_{\min}$	$\delta_{\max}$	$\delta_{\min}$	$\delta_{\max}$
$\boldsymbol{T}^u$	-0.200	0.200	-0.1194	0.1194	-0.7832	3.6114
$\boldsymbol{T}^p$	-0.200	0.200	-0.1189	0.1189	-1.6818	1.6818
$\boldsymbol{T}^u$	-0.3452	0.3452	-0.3759	0.3759	-0.7832	3.5925
$\boldsymbol{T}^p$	-0.6315	0.6315	-0.3760	0.3760	-1.6815	1.6815

TABLE II: $\delta_{\min}$ and $\delta_{\max}$ obtained by fixed point iteration for perturbations of Δ, J and γ for our quantum example. The nominal (unperturbed) values are $\Delta_0 = 0$, $J_0 = 1$ and $\gamma_0 = 0.01$ for rows one and two; $\Delta_0 = 0$, $J_0 = 1$ and $\gamma_0 = 0.1$ for rows three and four.

E. Quantum vs. mechanical systems

As already said, a limitation to passivity-control of lightly damped oscillatory mechanical systems is the co-location error between point of application of actuators and point of rate recording. Quantum systems also involve co-location at their core. In the single-particle Hamiltonian $H = \frac{1}{2}\omega_q \sigma_z$, the Pauli operator σ_z indicates that the qubit is subject to a magnetic field along the z-axis and measurements with possible outcomes spin up or down are relative to *exactly* the same magnetic field. Spin chains involve co-location errors, referred to as *bias spillage* [10] along the chain axis, conceptually similar to co-location error in space structures. A highly focused magnetic field meant to address a single spin always entails an error between the bias field and the spin it is

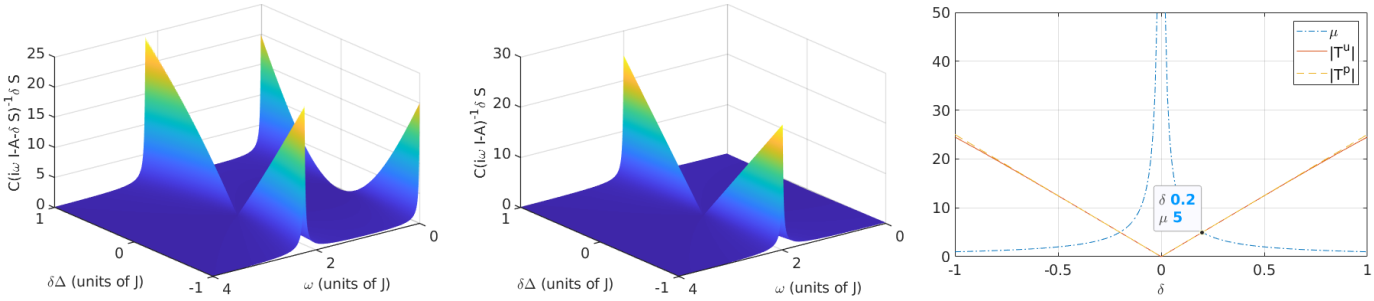

(a) Unperturbed Transfer function (b) Perturbed Transfer function (c) μ vs δ

Fig. 4: Transfer function relative to unperturbed and perturbed state and μ for uncertainty in $\Delta = \Delta_0 + \delta_{(\Delta)}$ with $\Delta_0 = 0$, $J = 1$, $\gamma = 0.01$. The intersection point of $\delta_{(\Delta)} = \mu(\delta_{(\Delta)})$ determines $\delta_{(\Delta),\max}$ and $\mu_{(\Delta),\infty}$.

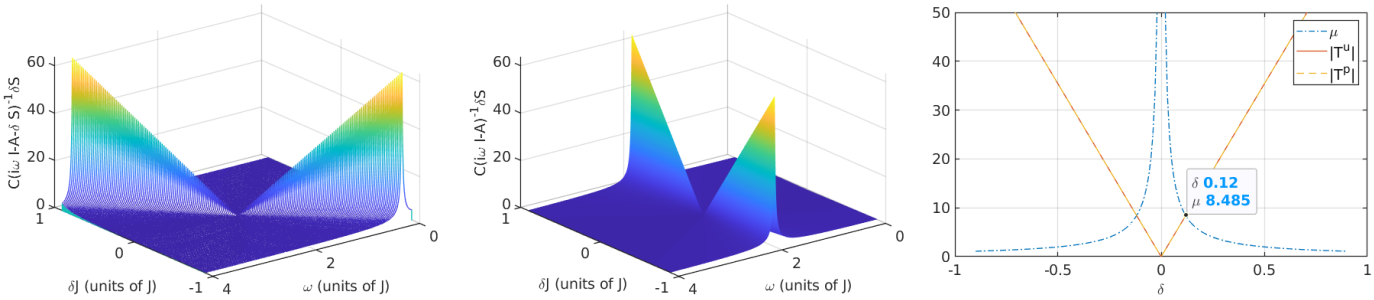

(a) Unperturbed transfer function (b) Perturbed transfer function (c) μ vs δ

Fig. 5: Transfer function relative to unperturbed and perturbed state and μ for uncertainty in $J = J_0 + \delta_{(J)}$ with $J_0 = 1$, $\Delta = 0$, $\gamma = 0.01$. The intersection point of $\delta_{(J)} = \mu(\delta_{(J)})$ determines $\delta_{(J),\max}$ and $\mu_{(J),\infty}$.

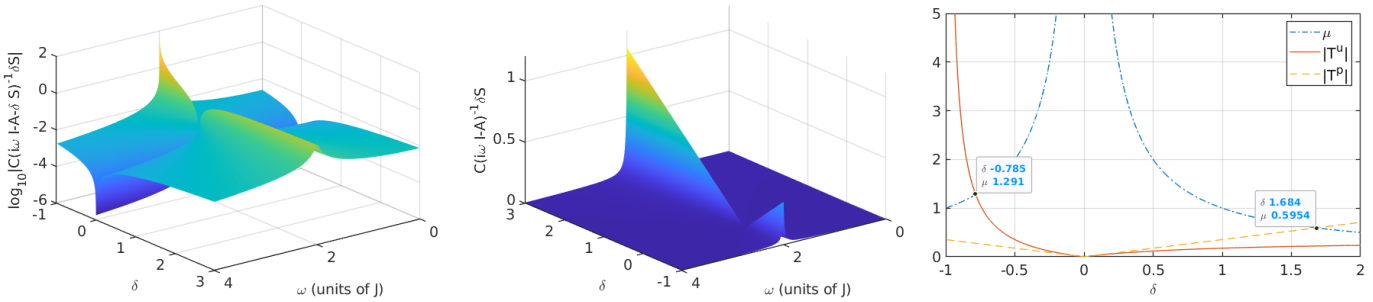

(a) Unperturbed transfer function (b) Perturbed transfer function (c) μ vs δ

Fig. 6: Transfer function relative to unperturbed and perturbed state and μ for uncertainty in $\gamma = \gamma_0 + \delta_{(\gamma)}$ with $\gamma_0 = 0.01$, $J = 1$, $\Delta = 0$. The intersection point of $\delta_{(\gamma)} = \mu(\delta_{(\gamma)})$ determines $\delta_{(\gamma),\max}$ and $\mu_{(\gamma),\infty}$.

supposed to address; a caveat that is well known in passivity control of distributed parameter space structures [15].

VII. Conclusion

The key point of this paper is that robust performance under structured uncertainties in both classical and quantum systems can be assessed independently of additive noise, which sometimes is physically legitimate but too often solely motivated by a textbook solution to assessing robust performance. If noise is legitimate, then the proposed approach has the advantage of homing in on the effect of the uncertain parameters independently of the noise.

Suppression of the noise is accomplished by removing the unperturbed dynamics from the perturbed dynamics leading to two different but equivalent error systems: one driven by the unperturbed dynamics, the other by the perturbed dynamics. From a design point of view, the unperturbed forcing term calls into question the relevance of the worst case, or H^∞, approach since the driving term is perfectly known, possibly resuscitating the old geometric disturbance decoupling problem. On the other hand, for the perturbed driven model, the H^∞ approach might still, in spirit, be appropriate since the disturbance is imprecisely known, yet not totally unknown. These design questions are left for further research.

Also left for further research is the development of a genuine

Brouwer fixed point substitute for the μ-function mandated by nonlinear uncertainties. All that has been done in this paper is to indicate how the fixed point solution could be implemented in the simple case of one uncertainty. Extension to multiple structured uncertainties calls for new mathematical control challenges.

REFERENCES

[1] V. Belevitch. *Classical Network Theory*. Holden-Day, San Francisco, 1968.

[2] H. W. Bode. *Network Analysis and Feedback Amplifier Design*. Van Nostrand, New York, 1945.

[3] Y. Dong, X. Meng, L. Lin, R. Kosut, and K. B. Whaley. Robust control optimization for quantum approximate optimization algorithm. https://arxiv.org/abs/1911.00789, 2019.

[4] M. Ezawa. Electric-circuit simulation of the Schrödinger equation and non-hermitian quantum walks. *Phys. Rev. B*, 100:165419, 2019.

[5] F. F. Floether, P. de Fouquieres, and S. G. Schirmer. Robust quantum gates for open systems via optimal control: Markovian versus non-Markovian dynamics. *New Journal of Physics*, 14:1–26, 2012. 073023.

[6] E. A. Jonckheere, S. G. Schirmer, and F. C. Langbein. Quantum networks: The anti-core of spin chains. *Quantum Information Processing*, 13:1607–1637, 2014.

[7] E. A. Jonckheere, S. G. Schirmer, and F. C. Langbein. Information transfer fidelity in spin networks and ring-based quantum routers. *Quantum Information Processing*, 14(10):4751–4785, 2015.

[8] E. A. Jonckheere, S. G. Schirmer, and F. C. Langbein. Jonckheere-Terpstra test for nonclassical error versus log-sensitivity relationship of quantum spin network controllers. *International Journal of Robust and Nonlinear Control*, 28(6):2383–2403, 2018.

[9] Y.-C. Liang, Y.-H. Yeh, P. E. M. F. Mendonça, R. Y. Teh, M. D. Reid, and P. D. Drummond. Quantum fidelity measures for mixed states. *Reports on Progress in Physics*, 82(7):076001, 2019.

[10] S. O'Neil, E. Jonckheere, S. Schirmer, and F. Langbein. Sensitivity and robustness of quantum rings to parameter uncertainty. In *IEEE CDC*, pages 6137–6143, 2017.

[11] PH. Opdenacker and E. A. Jonckheere. LQG balancing and reduced LQG compensation of symmetric passive systems. *International Journal of Control*, 41(1):73–109, 1985.

[12] PH. C. Opdenacker, E.A. Jonckheere, M.G. Safonov, J.C. Juang, and M. Lukich. Reduced order compensator design of a flexible structure. *Journal of Guidance, Control and Dynamics*, 13(1):46–56, 1990.

[13] Ian R. Petersen. Robustness issues in quantum control. In John Baillieul and Tariq Samad, editors, *Encyclopedia of Systems and Control*, pages 1–7. Springer London, London, 2013.

[14] P. Rooney, A. M. Bloch, and C. Rangan. Flag-based control of quantum purity for $n = 2$ systems. *Phys. Rev. A*, 93:063424, 2016.

[15] M. G. Safonov, E. A. Jonckheere, M. Verma, and D. J. N. Limebeer. Synthesis of positive real multivariable feedback systems. *International Journal of Control*, 45(3):817–842, 1987.

[16] M. G. Safonov, A. J. Laub, and G. L. Hartmann. Feedback properties of multivariable systems: The role and use of the return difference matrix. *IEEE Transactions on Automatic Control*, 26(1):47–65, 1981.

[17] S. G. Schirmer, E. A. Jonckheere, and F. C. Langbein. Design of feedback control laws for spintronics networks. *IEEE Transactions on Automatic Control*, 63(8):2523–2536, 2018.

[18] S. G. Schirmer, E. A. Jonckheere, S. O'Neil, and F. C. Langbein. Robustness of energy landscape control for spin networks under decoherence. In *IEEE CDC*, pages 6608–6613, 2018.

[19] S. G. Schirmer, F. C. Langbein, C. A. Weidner, and E. A. Jonckheere. Robustness of quantum systems subject to decoherence: Structured singular value analysis? In *IEEE CDC 2021*, pages 4158–4163, 2021.

[20] S. G. Schirmer, F. C. Langbein, C. A. Weidner, and E. A. Jonckheere. Robust control performance for open quantum systems. *IEEE Transactions on Automatic Control*, 2022. To appear; available at arXiv:2008.13691 [math.OC].

[21] S. G. Schirmer and Xiaoting Wang. Stabilizing open quantum systems by Markovian reservoir engineering. *Phys. Rev. A*, 81:062306, 2010.

[22] S. G. Schirmer, T. Zhang, and J. V. Leahy. Orbits of quantum states and geometry of Bloch vectors for N-level systems. *Journal of Physics A: Mathematical and General*, 37(4):1389, 2004.

[23] Y. Wang, H. M. Price, B. Zhang, and Y. D. Chong. Circuit implementation of a four-dimensional topological insulator. *Nature Communications*, 11:2356, 2020.

[24] B. Wie and D. Bernstein. Benchmark problem for robust control design. *American Institute of Aero. and Astro.*, 15:1057–1059, 09 1992.

[25] K. Zhou and J. C. Doyle. *Essentials of robust control*. Prentice Hall, Upper Saddle River, NJ, 1998.

Sophie Schirmer (Shermer) is an Associate Professor in Physics at Swansea University, UK, and previously held positions as Advanced Research Fellow of the Engineering & Physical Sciences Research Council at Cambridge University, Visiting Professor at Kuopio University, Finland, and positions at the Open University and University of Oregon. SS's research interests include nano-science at the quantum edge and quantum engineering, especially modeling, control and characterization of quantum systems.

Frank C. Langbein received his Mathematics degree from Stuttgart University, Germany in 1998 and a Ph.D. from Cardiff University, Wales, U.K. in 2003. He is currently a senior lecturer at the School of Computer Science and Informatics, Cardiff University, where he is a member of the visual computing group. His research interests include modeling, simulation, control and machine learning applied to quantum technologies, geometric modeling and healthcare. He is a member of the IEEE and the AMS.

Carrie A. Weidner received B.S. degrees in Engineering Physics and Applied Mathematics in 2010 and a Ph.D. in physics in 2018, all from the University of Colorado Boulder. Her Ph.D. work in JILA developed an interferometric sensing method using ultracold atoms in a phase-modulated optical lattice. After a stint as a postdoctoral researcher at Aarhus University, she is currently a lecturer in the Quantum Engineering Technology Laboratories, H. H. Wills Physics Laboratory and Department of Electrical and Electronic Engineering at the University of Bristol, where her current research focuses on methods and applications of quantum control and simulation.

Edmond A. Jonckheere received his Engineering degree from the University of Louvain, Belgium, in 1973, Dr.-Eng. in Aerospace Engineering from the Université Paul Sabatier, Toulouse, France, in 1975, and Ph.D. in Electrical Engineering from the University of Southern California in 1978. In 1973-1975, he was a Research Fellow of the European Space Agency; in 1979, he was with the Philips Research Laboratory, Brussels, Belgium, and in 1980 he joined the University of Southern California, where he is a Professor of Electrical Engineering and Mathematics and member of the Centers for Applied Mathematical Sciences and Quantum Information Science and Technology. He is a Life Fellow of the IEEE whose research interests include conventional vs quantum control, adiabatic quantum computations, wireless networking and the power grid.